# Indian Ocean Dipole in CFSv2 & ESMv1: Role of ocean biases

Thesis submitted for fulfilment of Training Program in Earth Systems Science

by

Shikha Singh

Center for Advanced Training

Indian Institute of Tropical Meteorology, Pune

Under the Guidance of

Dr Vinu Valsala

Dr(s) Swapna Panickal

Dr. Roxy Mathew Koll

Indian Institute of Tropical Meteorology, Pune

# CERTIFICATE

This is to certify that the work entitled ‘ Indian Ocean Dipole in CFS & ESMv1: Role of ocean biases’ being submitted by Ms. Shikha Singh has been carried out under our supervision, in partial fulfillment of the requirements for the Induction Training at CAT-ESSC, IITM. The matter embodied in this thesis has not been submitted for award of any degree in any University or Institute.

| | | |
|---|---|---|
| Dr. Vinu Valsala | Dr(s). Swapna Panickal | Dr. Roxy Mathew Koll |
| CAT-ESSC, IITM | CCCR, IITM | CCCR-IITM |

## Table of Contents

Abstract……1

Chapter 1: Introduction……3

1.1 Literature Survey……...6

Chapter 2: Data and Methods……..9

2.1 Data……9

2.2 Methodology……11

Chapter 3: IOD resolved in model simulations……..13

3.1 Validation of mean state of models with observations……13

3.2 IOD in models and observations……..24

Chapter 4: Role of biases in model IOD……32

4.1 Model Experiment……...38

Chapter 5: Relationship with monsoon……..54

Chapter 6: Discussion……60

Chapter 7: Conclusion……65

Chapter 8: References……67

## Abstract

Indian Ocean dipole (IOD) is a dominant mode of variability in the tropical Indian Ocean. There have been many studies on its evolution, triggering mechanism, life cycle and periodicity. The present study investigates the evolution of the IOD, specifically its intensity and frequency in two models, the NCEP Climate Forecast System v2 (CFSv2), and the IITM Earth System Model (IITM ESMv1). IITM ESMv1 is based on the CFSv2, but has an updated version of the ocean model (MOM4p1 instead of MOM4p0), and has been developed in-house at CCCR, IITM to study the attributions and projections of climate change and its impact on the global monsoon. Both the coupled models were integrated over 100 years, using similar initial conditions, in order to understand the role of subsurface oceanic biases on the evolution of IOD.

The dipole mode index (DMI) defined as in Saji et al., (1999) for both the models show high frequency spurious 'IOD-like' signals built in, with events in the earlier part of the year (Jan-May). The power spectrum analysis of both DMI and principle components of EOF-2 of SST show spurious peak at 9-10 months. We attribute the spurious IOD-like events to the oceanic biases in the model tropical regions and connected the deep ocean bias to the surface ocean dynamics via WKJB theorem. Brunt-vaisala frequency profile of both models was constructed and dominant baroclinic speed and its biases with respect to observations were estimated. It was found that both the models have a 'faster' dispersion of equatorial planetary waves than in the observations. This faster dispersion of equatorial waves is hypothesized to result in a mechanism, which we name as–'short term intensification of feedback'. According to this hypothesis, even in the absence of preconditioning, i.e. in the earlier part of the year (Jan-May), the increased dispersion of equatorial waves causes a 'faster' separation of temperature

anomalies in the east-west direction in the equatorial region, which amplifies the wind anomaly and leads to a SST-moisture negative feedback causing an oscillatory nature in the IOD time-series. The faster wave dispersion has been proved by sensitivity experiments conducted with a reduced gravity ocean model initialized with model and observed stratifications as well as forced with model and observed wind anomalies.

The correlation analysis between the DMI and monsoon is observed to be weak in both the models, as compared to the observations. The velocity potential and moisture transport anomalies in the low-level during IOD events in both the models show a significant reduction in low level convergence and moisture transport over the Indian subcontinent during positive IODs. The role of spurious IODs and its role on weak correlations of IOD and summer monsoon rainfall warrant further studies. The study points out the need to minimize the oceanic biases in climate models for better resolving dominant climate variability. Such biases could result in spurious inter-annual variability in the tropical regions in any climate simulation and that could be wrongly interpreted as induced by climate change.

## Chapter -1: Introduction

The El Niño-Southern Oscillation (ENSO) is well recognized as the most dominant climate signal at inter-annual to inter-decadal variability in the Pacific Ocean (Philander, 1990) and with significant tele-connection to other major basins (Su et al. 2001). For the Indian Ocean as well, the debate is that the dominant mode of inter-annual signal is ENSO itself (Gu and Philander, 1990, Trenberth 1997). However, the anomalous conditions that co-occurred in the Indian Ocean during certain years, which are arguably independent of ENSO, has been recognized as the second mode of  mode of variability in the EOF of sea surface temperature (SST) and called as the Indian Ocean Dipole mode (IOD), (Saji et al. 1999). This mode is characterized by warm SST anomalies in the western Indian Ocean and cold SST anomalies in the eastern Indian Ocean in its positive phase. The SST anomalies are accompanied by easterly wind anomalies in the equatorial Indian Ocean and alongshore of the Java-Sumatra coast. The sea-surface height remains lower than normal in the east and higher in the west. This pattern reverses during the negative phase of the dipole mode. The IOD is phase-locked to the seasonal cycle in the Indian Ocean, and the peak strength of the signal is observed during Sept-Oct, i.e. boreal fall (Annamalai et al. 2003) . The positive phase has the capacity to cause droughts in Indonesia, surplus rainfall over India and Australia and the east African (Saji et al. 1999; Webster et al. 1999).

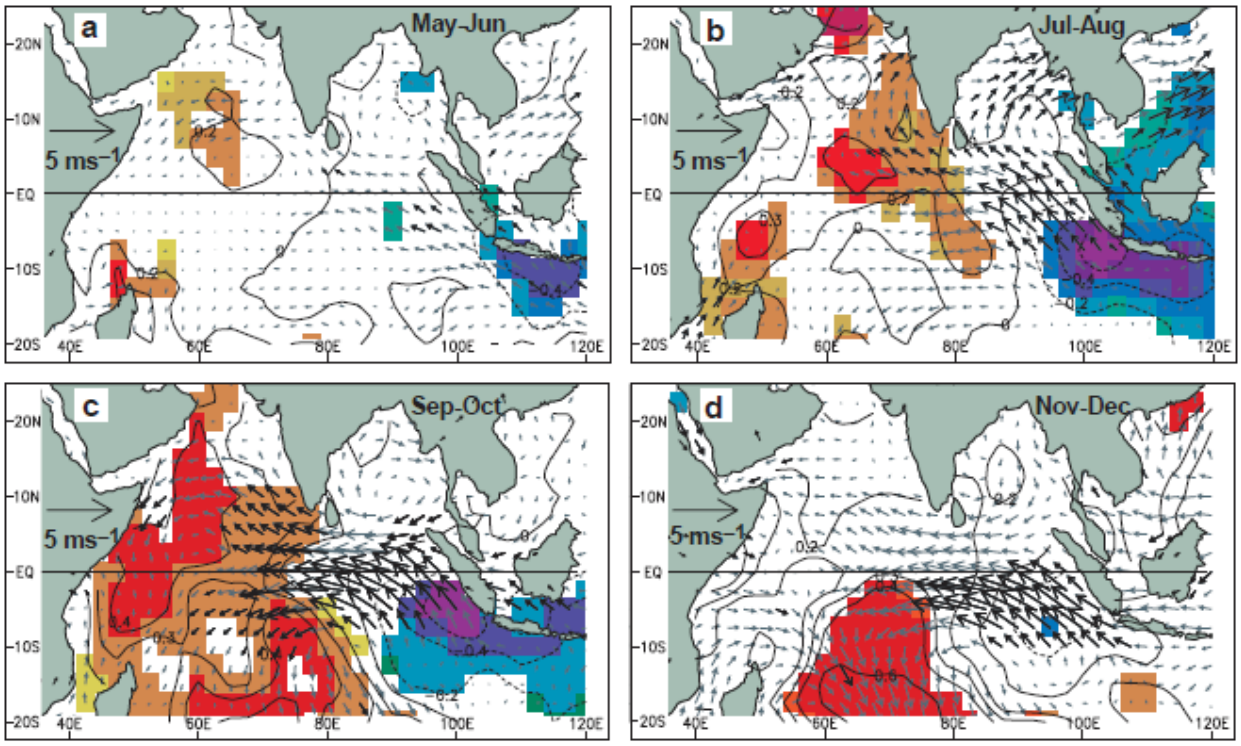


Fig 1: Composite of a positive IOD events as in Saji et al, (1999)

The Indian summer monsoon rainfall (ISMR) occurring during June-September contributes to more than 80% of country's annual mean rainfall and plays a crucial role on both agriculture and economy of the Indian subcontinent (Gadgil et al. 2004; Parthasarathy et al., 1994). It is known that a negative correlation exist between the anomalies of the ISMR and Niño-3 SST anomalies (area-averaged SST over 5°N-5°S and 150°W-90°W), however the overall correlation of El Niño and ISMR are below -0.4 (Kripalani and Kulkarni 1994). IOD, on the other hand, is positively correlated with ISMR. But the relationship between IOD and ISMR also depends on its independent or co-existence with ENSO. An above normal positive IOD year brings surplus ISMR despite the simultaneous action of ENSO(Saji et al. 1999; Webster et al. 1999). However this relationship has decadal modulation, there are epochs of IOD and ISMR 'grip' is stronger despite the action of ENSO (Ashok et al. 2004)

The accurate representation of IOD events in general circulation models is recognized as essential to simulate inter-annual variability of ISMR. The El-Niño is observed to have a negative correlation with the ISMR, but the coupled models sometimes fail to capture this relation (Achuthavarier et al. 2011) . In coupled models, the accurate representation of mean state of the atmosphere-ocean system is crucial for the models to have reasonable inter-annual variability and tele-connections. The biases in the mean state may affect the underlying dynamics and processes. Since the ISMR is having important role in the economy of the country, the accurate predictions of ISMR are vital and phenomenon such as IOD and its representations in the forecasting models becomes crucial. Moreover, reasonable simulations IOD in coupled models (Iizuka et al., 2000) are crucial for the further understanding of the IOD evolution and its possible deviations in the climate change(Cai et al. 2013).

Coupled Climate Forecasting System version 2 (CFSv2) has been proved to be an efficient dynamical forecasting tool of ISMR on seasonal and extended range predictions(Sahai et al, 2013). To be more specific, the Indian Institute of Tropical Meteorology (IITM) has adopted CFSv2 as the base tool for the 'seamless' prediction of the Indian monsoon. This tool is also the key ingredient of the National Monsoon Mission of Government of India). In addition to seasonal and extended range predictions of ISMR using CFSv2, the Center for Climate Change Research (CCCR) of IITM is restructuring this model for its climate predictions of hundreds of years from present. In this connection, the fidelity of the model to carry out simulations of hundreds of years has to be verified. The present study is aimed to validate the IOD and ISMR relations simulated in CFSv2 and its 'daughter' the earth system model (ESM, see chapter 2 for details) in a 100 year long free run from a common initial conditions.

## 1.1 Literature Survey

Latif and Barnett (1995) carried out several uncoupled and hybrid-coupled model experiments to demonstrate that while the air-sea interactions in the IO are weaker than those in the Pacific, they do contribute significantly to the local SST variability. Since then, (Saji et al. 1999) has identified the dipole, and many studies have been done on the Indian Ocean Dipole, the various effects and causes to understand it better. Saji et al,1999 defined the index as the difference in SSTA (DMI= SSTA (50°-70°E, 10°S-10°N) -SSTA(90°-110°E, 10°S-Eq), since there is strong correlation of this index with the PC2 of EOF on SSTA. In a series of studies (Yamagata et al. 2003), there have been methods to verify the existence and dominance of the phenomenon. The independence of this dipole mode from the ENSO in Pacific Ocean has been discussed for a long, but since IOD has seen to evolve and persist even in the absence of El-Niño it is clear that it is not totally dependent on ENSO. (Fischer et al. 2005) suggest triggering mechanisms, as the anomalous Hadley circulation when no ENSO, and the anomalous Walker Circulation when ENSO is co-occurring.

The influence of an ongoing IOD on a developing El-Niño is studied. (Annamalai et al. 2004) reports that circulation anomalies induced by Indian Ocean heating anomalies can modulate the ongoing El Niño, by affecting SST variance in the Pacific. (Izumo et al. 2010) states that the Indian Ocean Dipole modulates the strength of the Walker circulation in autumn. The quick demise of the Indian Ocean Dipole anomaly in November–December then induces a sudden collapse of anomalous zonal winds over the Pacific Ocean, which leads to the development of El Niño/La Niña. And this can be used to forecast ENSO well in advance.

On the various characteristics of phenomenon, (Vinayachandran et al. 2002) study the seasonal evolution of the IOD events in the Indian Ocean by analyzing both surface and surface signatures from an ocean model simulation and the observations. They also identify the role of Rossby and Kelvin waves in the lifecycle and duration of the mode. How the easterly wind anomalies excite an upwelling Kelvin wave in the equatorial IO & this Kelvin wave reflects primarily as a first baroclinic mode upwelling Rossby wave has been explained (Vinayachandran et al,2002; Murtugudde et al,2000, Valsala, 2008).

The impacts of the IOD on a global scale as well as with respect to the monsoon is a part of various studies (Saji and Yamagata 2003; Ashok et al. 2001; Rao and Yamagata 2004; Vinayachandran et al. 2006; Zheng and Xie 2009). These studies suggest that, the phenomenon affects not only the entire system through tele-connections; it also has relationship with small intra-seasonal scale processes. In a series of papers Ashok et al., (2001, 2003b, 2004a) in which the relationship of IOD and Monsoon is discussed. Some key points of the study are that IOD variability during each month of July to September apparently contributes more to JJAS rainfall as compared to that during June, probably because IOD is still in pre development stage in June. However, if the IOD signal is strong by June, we see a wider impact of the IOD even during that month. IOD events have maximum impact around the monsoon trough areas, and a few parts of the west coast. Positive IOD events, in particular, seem to accentuate the active monsoon-like conditions. When analyzing the relationship b/w the ISMR and ENSO, in presence of an IOD, it states that the anomalous ENSO-induced subsidence over the Indian region that normally occurs during the 'ENSO only' years is replaced by the IOD-induced convergence; this leads to the normal JJAS monsoon rainfall even during strong El Niño years. The colder SST anomaly in the eastern tropical Indian Ocean causes reduction in convection during the positive IOD event and

so there is anomalous subsidence and divergence at the 850 hPa. Over the Bay of Bengal, on the other hand, convergence takes place in the lower troposphere due to the enhanced meridional circulation at lower levels. This causes anomalous intensification of the monsoon meridional circulation in the troposphere during the positive IOD event.

Considering the importance of IOD in climate, we focus to evaluate them in the CFSv2 and ESM. This topic deserve attention because the climate models such as CFSv2, which is originally designed for short-term simulations, taken to longer time scales of 100 or 200 years of climate simulations, one need to know its integrity in representing the mean climate even after it deviates from the initial conditions. To be more specific, the coupled models known to exhibit oceanic biases both in the surface parameters and in the deeper ocean profiles (Delworth et al. 2006). In such cases the interior biases may have influence on the surface representations of IODs in the model. Therefore, it becomes crucial to evaluate the oceanic inter-annual variability in these models and its relation to ISMR. In the case of ESM, this verification is essential because it serves as a validation component for the ESM, which is originally developed in CCCR.

In this aspect, following questions are found worth examining.

1. Evaluation of the IOD in hundreds years of climate model simulations using CFSv2
2. Evaluation of the IOD in ESM developed in CCCR
3. Examination of the role of oceanic biases in the evolution of IOD

The model design, experiment and analysis are given in chapter 2. The major results are given in chapter 3 and 4. A discussion based on our findings is offered in chapter 5. Results are summarized in chapter 5.

## Chapter-2: Data and Methods

### 2.1 Data

#### 2.1.1 Climate Forecast System version 2 (CFSv2)

The Climate Forecast System (CFSv2) is a fully coupled ocean–land–atmosphere-sea ice model from the National Centre for Environment Prediction (NCEP), with significant improvements since its first version (CFSv1) (Saha et al. 2010). This version of the CFSv2 is similar to the version of the NCEP model used for the climate forecast system reanalysis (CFSR) (Saha et al. 2010). The atmospheric component of the CFSv2 is the NCEP Global Forecast System (GFS) model. It adopts a spectral triangular truncation of 126 waves (T126) in the horizontal (*0.9° grid) and a finite differencing in the vertical with 64 sigma-pressure hybrid layers. The convection scheme employed in GFS is the Simplified Arakawa-Schubert (SAS) convection, with cumulus momentum mixing and orographic gravity wave drag (Saha et al. 2010). The ocean component is the modular ocean model version 4p0d (MOM4p0d), from the geophysical fluid dynamics laboratory (GFDL), which is a finite difference version of the ocean primitive equations configured under the Boussinesq and hydrostatic approximations. The zonal resolution is 0.5° and the meridional resolution is 0.25° between 10°S and 10°N, becoming gradually coarser through the tropics, up to 0.5° pole ward of 30°S and 30°N. There are 40 layers in the vertical with 27 layers in the upper 400 m, with a bottom depth of approximately 4.5 km. The vertical resolution is 10 m from the surface to the 240 m depth, gradually increasing to about 511 m in the bottom layer. The atmosphere, ocean, land and sea ice exchange quantities such as the heat and momentum fluxes every half an hour, with no flux adjustment or correction. The

CFSv2 model is time integrated over a period of 100 years, and the simulated daily data for the last 30 years (60-89) is used in the present study for the current analysis.

### 2.1.2 Earth System Model (ESM)

The ESM is indigenous design of Earth System Model by Center for Climate Change Research (CCCR) of IITM. It is aimed to provide simulations of climate change under various emission scenarios as in IPCC AR5 (IPCC 2013). In the nut-shell the CFSv2 givens the dynamic core of atmosphere, while ocean model MOM4p0d is replaced with MOM4p1 which has built-in biogeochemical ocean model known as TOPAZ (Dunne et al. 2005). Except for this difference the CFSv2 and ESM are same. An aerosol module, interactive land processes and ecosystem are currently under development. These additions are not used in the present study.

### 2.1.3 Initial conditions and length of simulations

Both CFSv2 and ESM are simulated with initial conditions given for the year of 2010 taken from the GODAS (oceanic) and NCEP (atmospheric) reanalyzes. Simulations are carried out for 100 years from the initial conditions. The model years from 60 to 89 spanning 30 years are used for the analysis. For analysis purpose, model outputs are produced as monthly averages centered at 15nth of each month.

### 2.1.4 Observations

For the validation purpose of CFSv2 and ESM simulations, we use a suite of observational data product. We used SST data from ERA Interim (Dee DP et al, 2011)

precipitation data from GPCP (Adler et al, 2003), and surface winds from NCEP (Kalnay et al, 1996). The oceanic re-analysis from SODA (Carton and Giese, 2008) is used for the oceanic variables. All the observations are used from 1983-2012 in order to mimic a 30-year span of the data which is similar to the length of the simulations analyzed, except for SODA, for which the data from 1972-2001 is used.

### 2.2 Methodology

Monthly climatology is constructed for all the variables. Monthly anomalies are generated by subtracting the climatology from the raw data. The DMI index as defined in (Saji et al. 1999) is calculated, DMI= SSTA (50°-70°E, 10°S-10°N) -SSTA(90°-110°E, 10°S-Eq).

#### 2.2.1 Power Spectrum Analysis

Power spectrum analysis of a time series gives information about the most dominant signal. It is calculated by simply taking Fourier Transform of the data, the Fourier transform separates the dominant signals, and tells the frequencies at which they are significant.

$$\widetilde{y_k} = \sum_{j=0}^{N-1} \left( y_j \exp \frac{2\pi i j k}{N} \right)$$

The same for the DMI data was carried out for retrieving the dominant power and its periodicity. We apply discrete Fourier transform to convert the data into frequency domain, and multiply the amplitude and frequency, to get a variance preserving spectra, which highlights only dominant frequencies giving them a shoot up.

### 2.2.2 Empirical Orthogonal Function Analysis

To examine spatially and temporally linked variability of ocean variables, we chose to use empirical orthogonal functions (EOFs). This method has been detailed previously in many papers (Kundu and Allan, 1976; Servain and Legler 1986). EOFs provide a series of ranked eigenvectors, each of which contains a percentage of the temporal variability of the data. Eigenvectors with the largest percentages are usually associated with physical processes. Each empirical orthogonal function consists of a spatial pattern modulated by an associated time series. To realize the original data at a particular time, as expressed by an individual EOF, the EOF pattern must be multiplied by the corresponding value of its associated time series. EOF analyses can therefore provide a set of basis functions representing the linked spatial and temporal variability of the data.

The results of the EOF for a single field give the dominant mode for that only, but the coupled/multivariate analysis identifies only those modes of behavior in which the variations of the two fields are strongly coupled. The method simply takes all the variability and breaks it into a few standing oscillations and a time series to go with each oscillation. Each of this oscillation is then referred as the mode of variability, and the principal component shows how it oscillates in time.

### 2.2.3 Composite Analysis

The composite is simply the average of all similar events to give a clear picture of the situation. All the uniform events are clubbed together and, a mean picture is identified.

# Chapter 3: IOD as resolved in model simulations

## 3.1 Validation of mean state of CFSv2 and ESM with observations.

We begin the analysis by examining the mean state of the model, and comparing it with the observations. It is important for the models to capture the background state, which is crucial for a better prediction of the model. Large-scale fluctuations of the tropical ocean noticeably affect variations of climate in the low-latitude regions. We begin the presentation of results first by focusing on the mean state of surface as well as subsurface ocean resolved in the 100 year long simulations of both the models and comparing them with the observations. The mean state of the models is evaluated as the 30-year average of the data from model year 60 to 89.

Figure 2 shows the global average of SST (annual means) from the initial condition to the end of the simulation. Both the model has initial cooling of surface temperatures for the first 30 years and then reaches a quasi-stead evolution. At the end of 100 year evolution both the models has a positive growth in global mean SST. The spin-up of these models are not complete in the first 100 years and a stationary state in ocean-atmosphere system may achieve only after several hundreds of years. However, the computational requirements limit us to first 100 year simulation and evaluate the state of the model.

Climate simulations are susceptible to oceanic biases in the vertical structure (Delworth et al., 2011). In order to look into the subsurface bias in CFSv2 and ESM, a simple temperature profile was plotted for observations, CFS and ESM up to a depth of 4000m, as basin averages over 50°E-110° E, 10°S-10°N (Fig 3). The temperature profile shows that there is cold bias at the surface in both the models, but at depths around thermocline, ESM has a larger warm bias

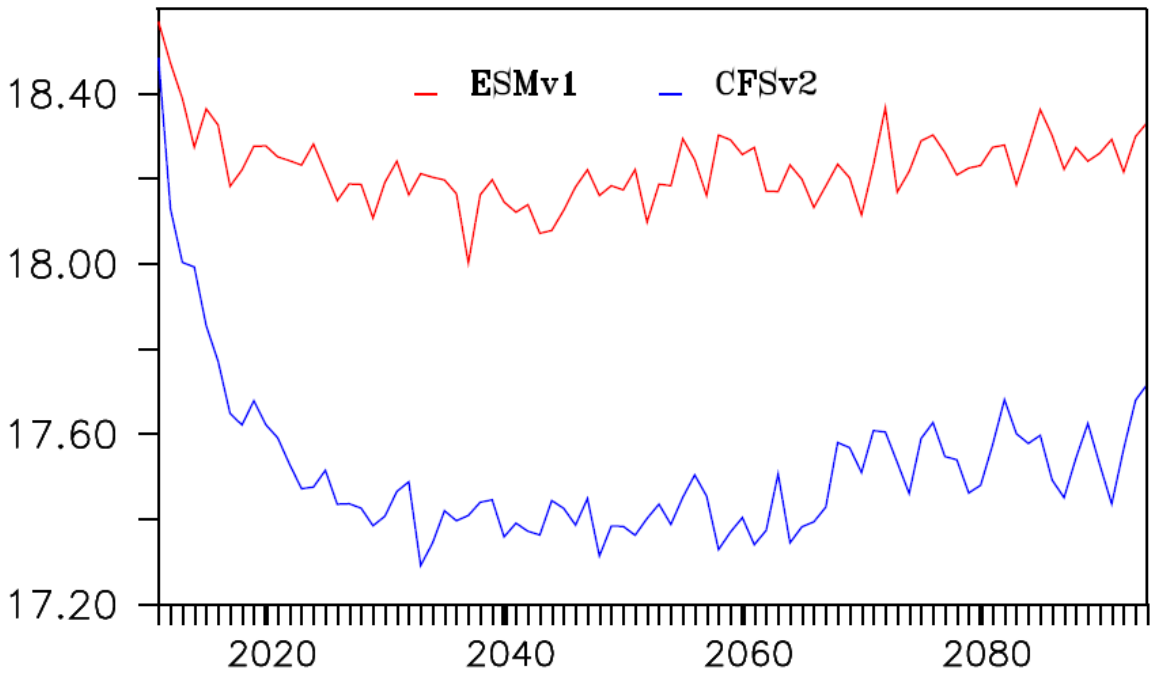


Fig 2: Evolution of global average sea surface temperature in the CFSv2 and ESM for the 100 years of model simulation

.

than CFS. At a depth of 200m, there is a bias of 5°C in ESM compared to 3°C in CFS. But after a depth of 950-1000m the temperature in ESM become almost equal to the observations, however, CFS still has a warm bias up-to the depth of ocean.

It is observed that the cold bias at the surface in CFS seems to be improved in ESM, but just below the surface layer, warm bias starts building up in both the models. Near the thermocline, where sharp temperature gradients occur, the warm bias in CFS is less than as compared to ESM. However, after a depth of about 1000m, the temperature profile of ESM very well matches with the temperature profile of observation, whereas there is still a warm bias present in CFS, which goes up to deep down the ocean even up to 3000 meters.

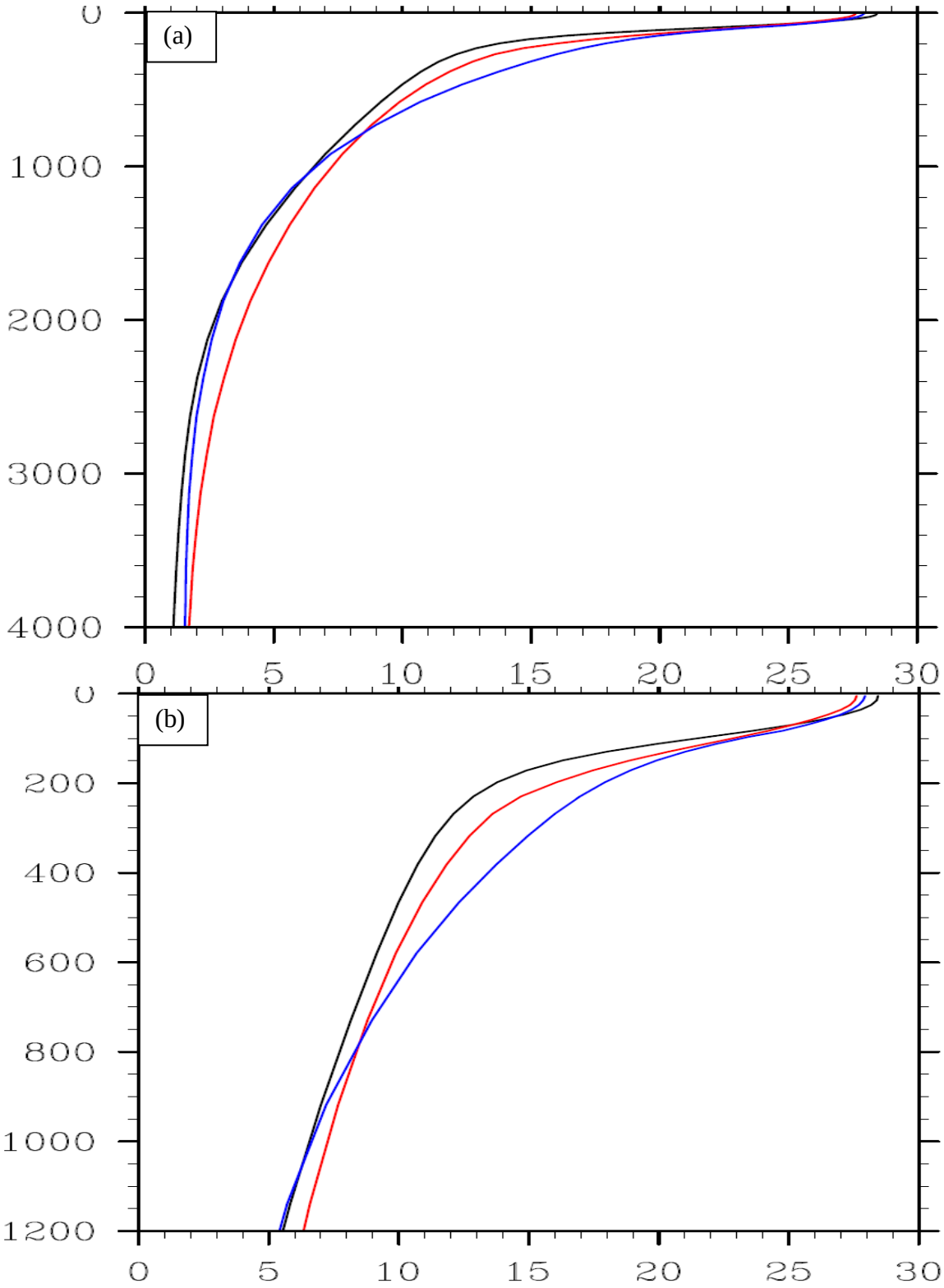

Fig3: Temperature profile. Black – Obs, Red – CFS, Blue – ESM, (b) zoomed 0-1200m.

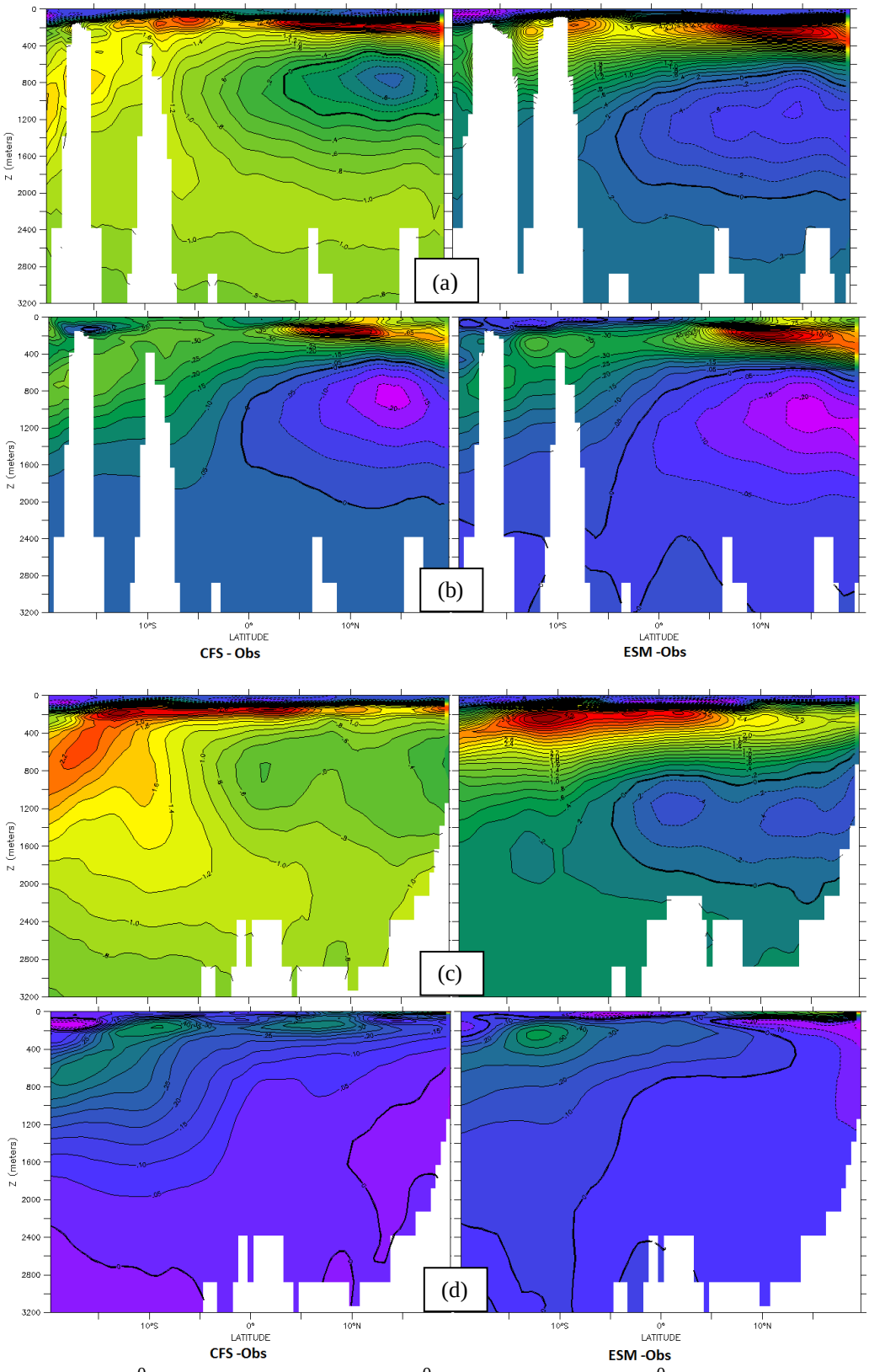


Fig 4: (a) $60^0$E temperature bias (b) $60^0$E salinity bias (c) $90^0$E temperature bias (d) $90^0$E salinity bias. The left panel shows (CFS-Obs), and the right panel (ESM-Obs).

In order to examine the vertical structure of the mean state of the model, a vertical section of both temperature and salinity bias is seen at 60°E and 90°E. The reason behind choosing these two longitudes is that one of them is in the west IO cutting through the Arabian Sea whereas the other in east IO cutting through the Bay of Bengal.

The western Indian Ocean, the temperature bias seems to be more surfaces trapped in both CFS and ESM. In the case of CFSv2, the bias seems to 'intrude' in to the oceanic interior rather from the south of $30^0$S. In the case of ESM, the deep cold core biases are centered around equatorial region and at a depth of 1000m. In the case of CFS, the cold bias is comparatively shallower at a depth of 800m. The salinity biases in both the model seem to have similar structure, with noticeable differences in the thermocline salinities of CFS, which is more saline than in the ESM as well as observations.

The $90^0$E shows that the cold core bias in the deep is diminished in both the models. The intrusion of warm biases from the southern latitude to the ocean interior in the CFS is more visible in the $90^0$E. This could be the model limitations in the mode-water representation, most of which subducts and advects to the northern Indian ocean through subsurface pathways(Schott and Jr 2001)

The dynamics governing coupled phenomenon such as IOD may not only depend on the surface features and air sea interaction but also may depend on the deep ocean structure. Considering the ocean as a continuously stratified fluid, the governing dynamics can be separated into certain sets of Eigen modes in the normal mode theory of the ocean wave-guide bounded between free-surface and deep ocean floor (Gill, 1982). Relating the deep ocean biases especially in the tropical regions that exist in both the model to the surface air-sea coupled

phenomenon such as IOD is the essence of this work. In order to achieve this, we first analyzed the thermocline and dynamic height variability of the model and compared them with the observations. This will give a first insight into the role of subsurface oceanic biases in the surface ocean dynamics resolved in both the models.

Thermocline is the depth at which the vertical temperature gradient is highest. The temperature takes a sharp bend from here and that separates the upper ocean from the deep (Fig 5). Above the thermocline, the warm temperatures are present as compared to that below thermocline. It is understood that the ocean layer above the thermocline participates in air sea interactions. The water below thermocline may enter to the upper ocean via upwelling and entrainments which has influence on surface ocean temperature and air-sea coupling. The vertical processes that affect the thermocline are downward or upward transfer of heat from the sea surface via processes such as upwelling, downwelling and entrainment. For the purpose of calculation, we took the 20°C isotherm depth as the base of the thermocline which is a suitable choice for the warm tropical ocean. Further, in order to show the dominant variability of model thermocline, we have used the EOF thermocline anomalies.

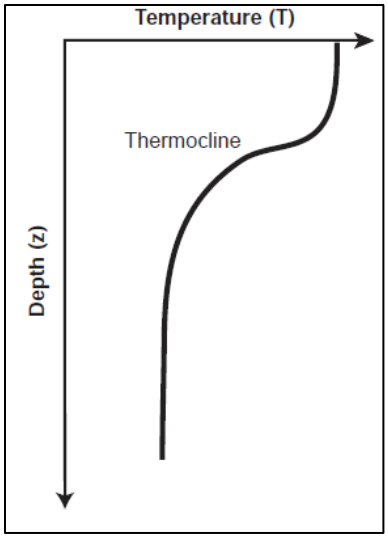


Figure 5: The schematic depicting thermocline

The spatial plots show that dominant mode of variability in thermocline is that of dipole mode in the observations (Rao et al., 2002, Deep Sea Res). So it can be said that the El-Nino based basin wide warming (mode 1 of EOF of SST), is limited only to surface. CFS simulates the thermocline dipole quite realistically. However, in ESM it is the second mode which shows the dipole mode, similar to observation and CFS mode 1. (The mode-1, however shows a trend like time-series which will be discussed later). The spatial structure shows clearly that the coastal Kelvin waves, and the Rossby waves moving towards west. The Rossby wave shows a tilted structure, which is expected due to the latitudinal dependence of speed of Rossby wave, whose speed decreases with increase in latitude.

The thermocline EOFs can represent only the upper ocean characteristics. In order to see whether the deep ocean biases reflected in the surface ocean dynamics we also looked at the dynamic height EOFs.

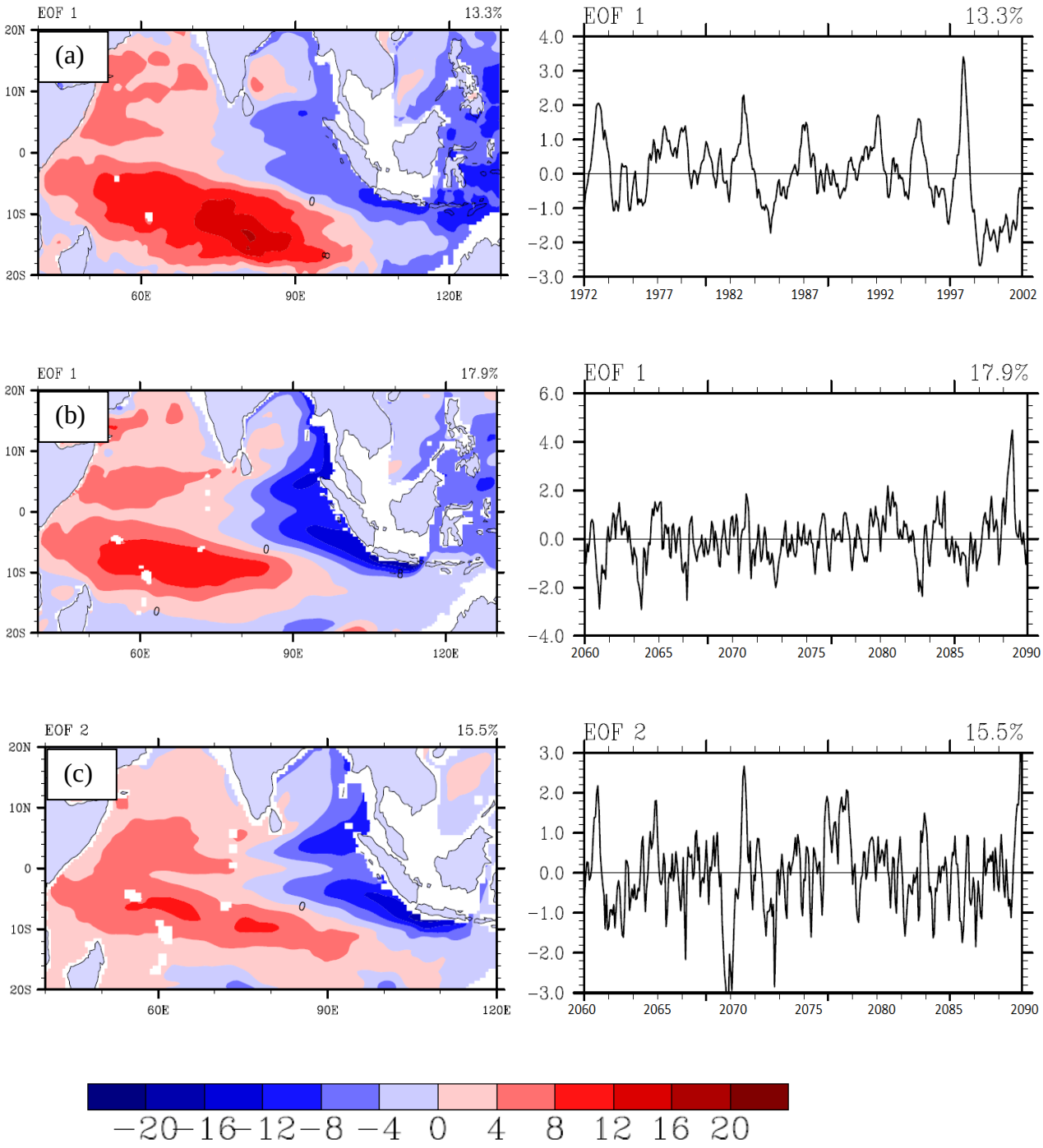


Figure 6: The spatial plots and respective PCs for EOF for thermocline (a) Observation mode 1 (b) CFS mode 1 (c) ESM mode 1.

Dynamic height is the amount of work required to move a unit mass of water vertically from sea level to a given point. Or, the gravitational potential energy per unit mass, just as geo-potential height in the atmosphere. It refers to the pressure associated with a column of water. Horizontal variations of dynamic height (due to horizontal variations in temperature and salinity) are mapped to determine what is called the dynamic topography and its corresponding geostrophic flow field in the ocean. The dynamic height is measured in dynamic meters and is defined by

$$D(p_1, p_2) = \int_{p_1}^{p_2} \delta(T, S, p) dp$$

where '$p_1$' and '$p_2$' are two reference pressure levels, 'δ' is the specific volume anomaly, 'T' is temperature, 'S' is salinity and 'p' is pressure. The unit is J/kg. It is not to be confused by 'height'. It is just a name given to gravitational potential energy per unit mass. Dynamic heights are preferred over geometric heights in ocean because energy is generally lost or gained when a parcel of fluid moves along a surface of equal geometric height but not when it moves along a surface of equal dynamic height.

We calculated the dynamic height from the model temperature and salinity. A dynamic height anomaly is further constructed and EOF is employed over it. The spatial plots show the observational plot as the dipole mode, explaining around 17% of variance, this mode appears as 2$^{nd}$ mode of variability in CFS, and explains ~5% of variance. Again, in the case of ESM, this appears as the first mode, where the variance explained is 34%.

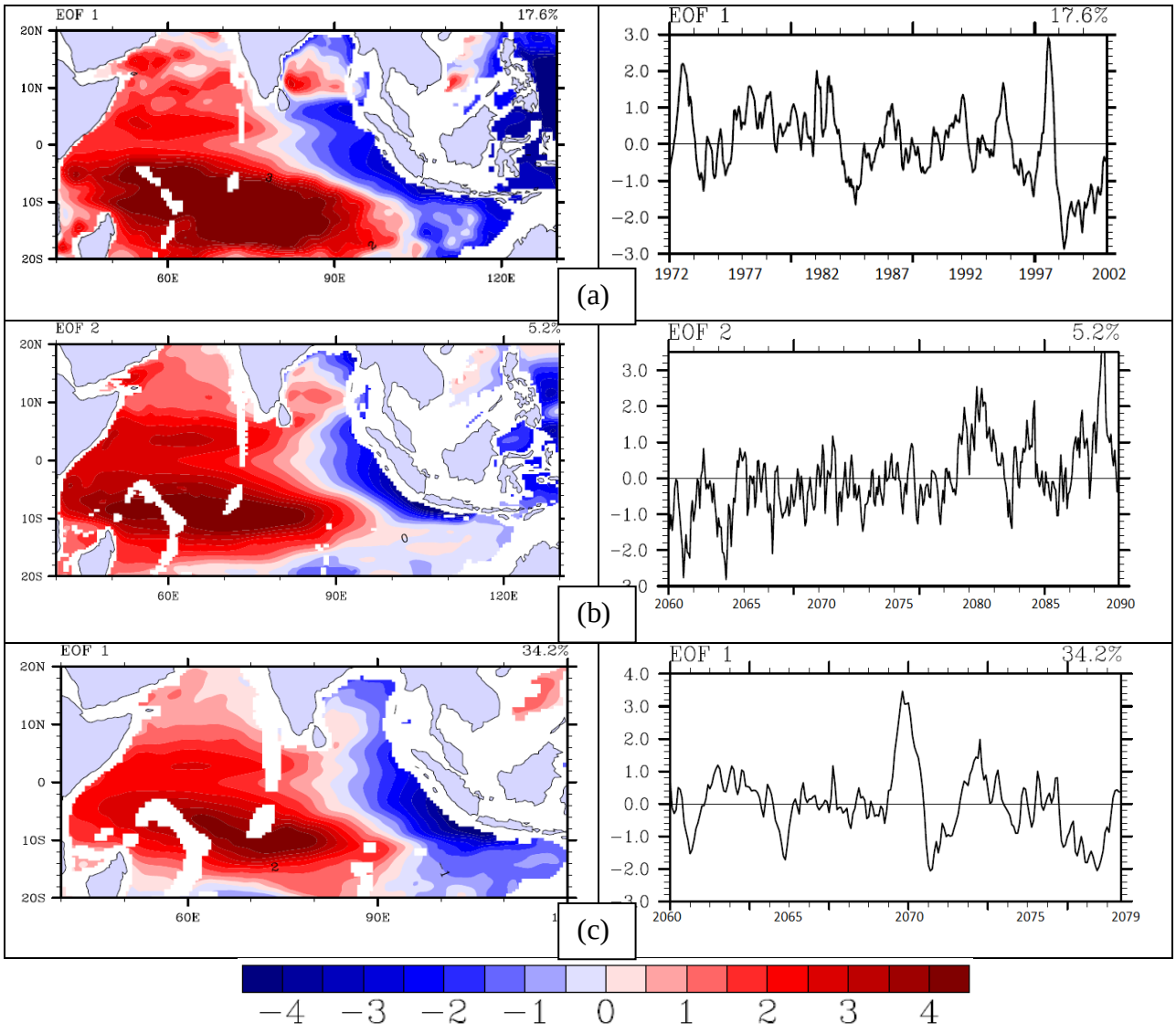


Figure 7: EOF of dynamic Height (a) Observation mode 1 (b) CFS mode 2 (c) ESM mode 1

The EOF analysis reveals that dominant mode of variability in thermocline and dynamic height for ESM and CFS, respectively, is not present in any mode of the observations. The thermocline of EOF-1 of ESM shows a basin wide increase in the thermocline depth and its principal components (PC) of suggest an increasing trend. This probably corresponds to building of biases at the thermocline. In the case of CFSv2, the dynamic height EOF-1 shows similar basin wide pattern and increasing trend in PC time series. These two disparities show that the

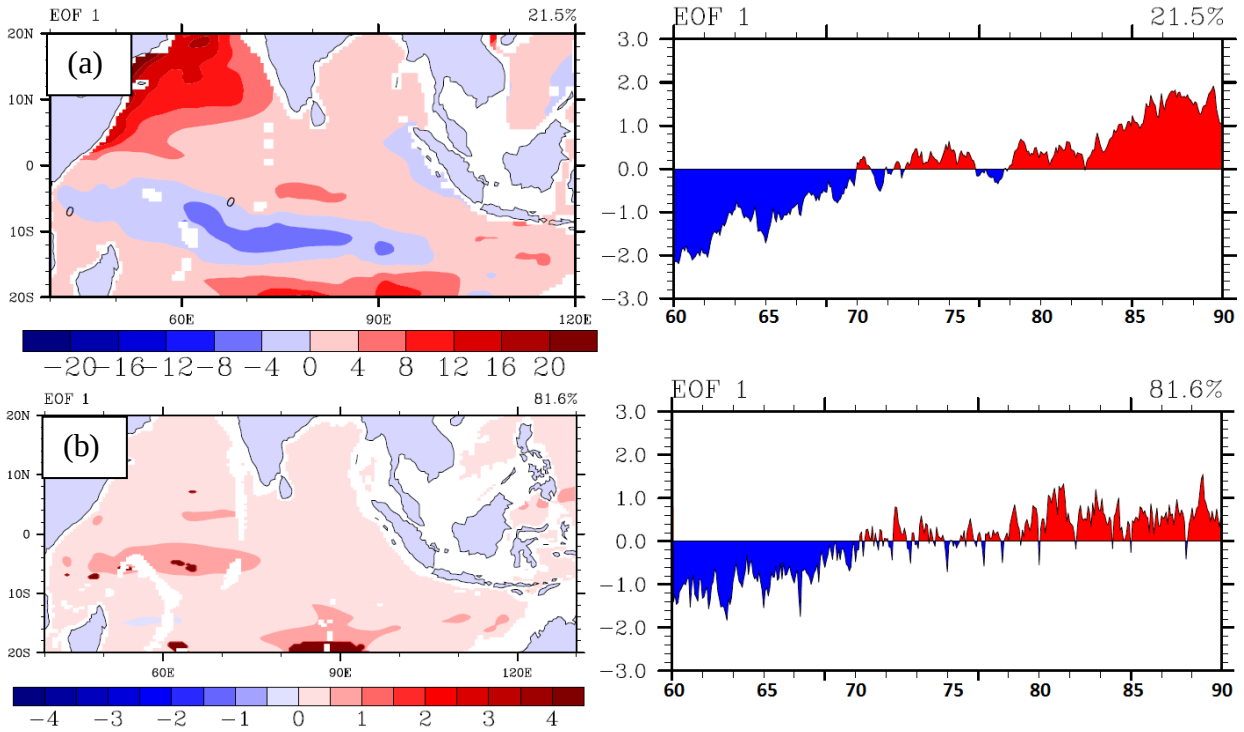


Fig 8: EOF mode 1 spatial plot and PC for (a) Thermocline in ESM & (b) Dynamic Height in CFS.

deeper ocean is still evolving in both the models in terms of biases and the effect of which can be further amplified for longer term simulations (over 100 years). The role of such spurious biases in the surface ocean dynamics requires a more serious attention. The essence of this work is to examine the relation between model simulated IOD and role of these deep ocean biases. Before proceeding to this topic, next we present the IOD as simulated in both CFSv2 and ESM and compare them with the observations.

These plots are pose a question, whether these building biases have a role to play in the ocean dynamics.

## 3.2: IOD of models and observation

As a validation purpose, here we present the results as a combination of CFSv2, ESM and observations. We calculated the monthly climatology and monthly anomalies of each data set for further analysis. The DMI index (Saji et al. 1999) is calculated from the SST anomalies. The power spectrum analysis is performed on the calculated DMI series. The power spectrum of DMI index is a possible way of IOD periodicity analysis as illustrated in (Ashok 2003)

The Fig. 9 shows the power spectrum of DMI for observation, CFS and ESM for a 30 year period. It can be seen that there is significant power in the CFS signal at 9-10 months period. The observation shows highest power at 30-40 month, which is identified as the dipole signal. The ESM shows highest power at the same period as of CFS, which is 9-10 months but the power of signal is comparatively less for all mode of variability. On the basis of the dominant periodicity obtained, it is seen that in both the models, there is some intermittent signal which is creating IOD like signals on a high frequency.

In order to observe the dipole events throughout the whole period of data, especially their evolution, decay and the life cycle, a matrix is created, where all the months with DMI > 1σ (σ = standard deviation), are shown in red, and DMI < 1σ are shown in blue (Fig 10). The standard deviation for each data is calculation from DMI of each dataset. The matrix shows that the lifecycle of IOD in the models is captured quite well and similar to the observation especially in the summer monsoon season. The event starts in May-June, peaks in September and decays by Oct-Nov. But the significant difference visible from the matrix is that there are a few early events in both the models. Observation matrix does not have them. It is important for us to look

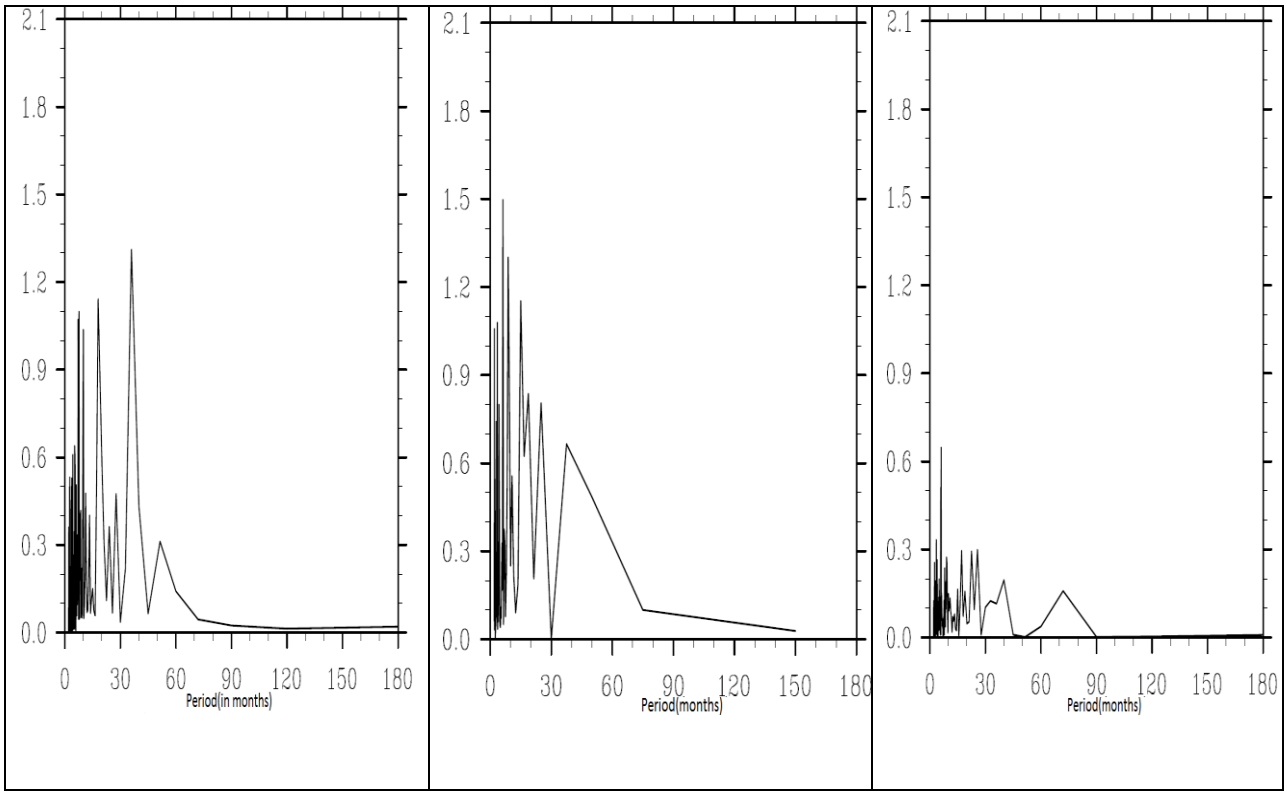


(a) (b) (c)

Figure 9: Power spectrum of DMI time series. (a) Observation 1972-2001 (b) CFS (c) ESM. X-axis shows period (months), and Y axis has power x frequency.

for the cause of these, as all such events are greater than 1 standard deviation and some of them stays longer than 2-3 months. This long period is sufficient for coupled ocean-atmospheric phenomenon to be positively fed-back and grow spontaneously. Such coupled mode may also serve as genesis for an IOD. Therefore identifying the cause of such off-season IOD-like "noises" in the model becomes important.

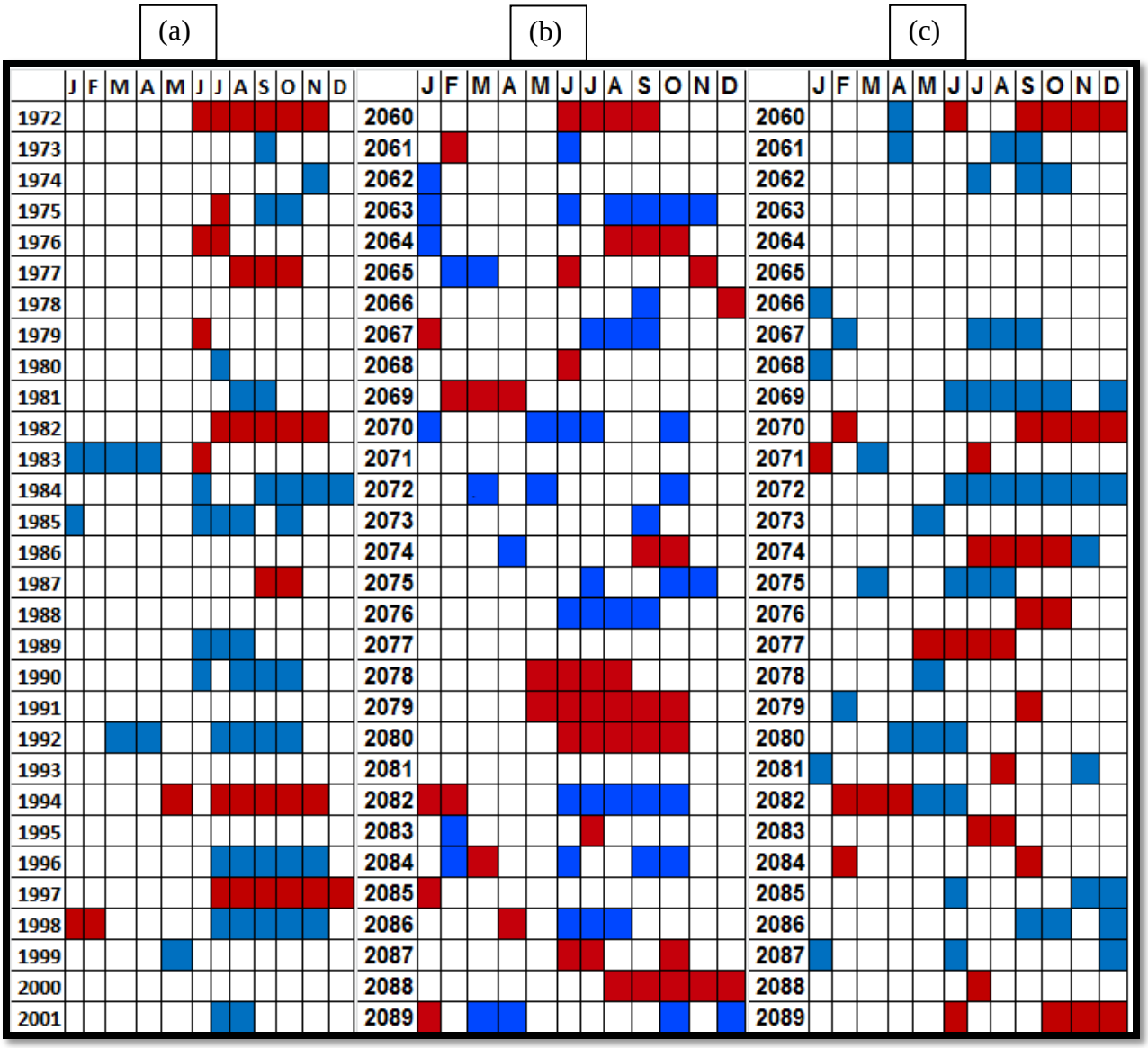


Figure 10: The matrix showing the months with DMI >1σ (red) and DMI<1σ (blue). (a) observation, (b) CFS and (c) ESM

**1.2 EOF analysis of surface parameters.**

In order to see how well the models have simulated the dipole, an EOF analysis is done for the SST over the Indian Ocean (40°E-110°E, 20°S-20°N). Fig 11&12 show the EOF SST spatial plots and the corresponding principal components. The EOF-1 shows a basin wide warming signal, as is present in observation. Such basin wide responses on inter-annual

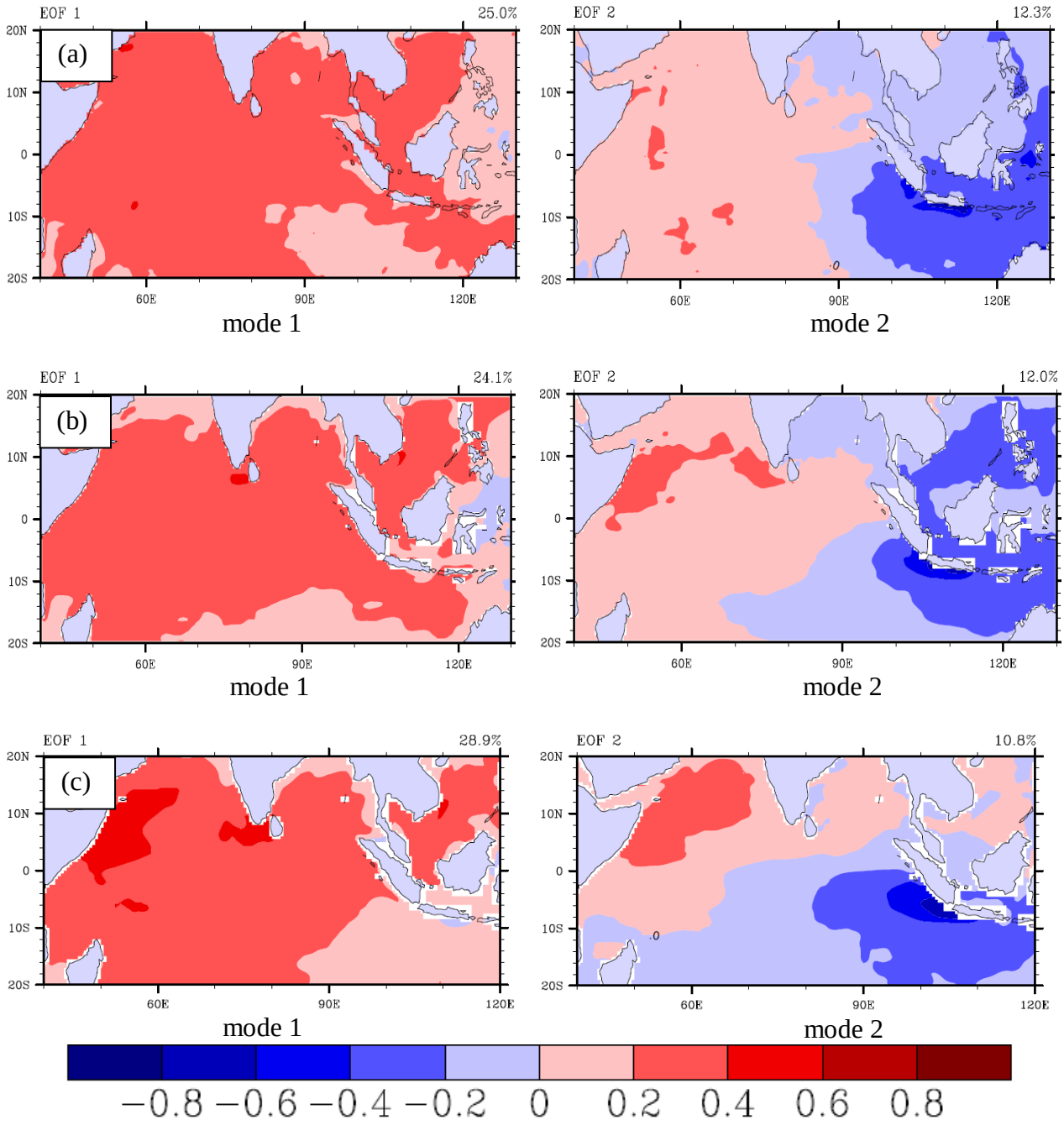


Figure 11: Spatial plots of EOF of SST, mode 1 and 2. (a) Observation 1972-2001 (b) CFS, model years 60-89 (c) ESM, model years 60-80.

scales are due to El Niño forcing (Saji et al. 1999). The first mode explains about 24% in CFS, and 29% in ESM, which is similar to 25% in observation.

The second EOF mode, which is the dipole mode, has been quite well simulated in CFS, but in ESM the west Indian ocean warming region seems to be shifted more into the Arabian sea basin. Variance explained is again similar, with 12% in CFS, 11% in ESM, and 12% in observation. Hence spatially and statistically, the models simulate the SST dipole quite reasonably.

The principal components of EOF-2 from CFS and to some extent from ESM are rather 'noisy' with intermittent positive and negative oscillations of EOF-2 type pattern within every 9-10 months. This feature was also obvious in the power spectrum analysis which has shown the high-frequency power close to this periodicity. It is anticipated that the noisiness might be arising due to those early events in the matrix shown in Figure 10.

The principal components of mode 1 are correlated with Nino 3.4 index, and CFS & ESM give a high correlation of 0.42 and 0.5 respectively, which in observation is 0.57. The mode 2 is correlated with DMI and correlation values as high as 0.74 and 0.83 are obtained both for CFS and ESM, as compared to 0.8 in observation. So the models also have the dominant mode of variability as the ENSO mode for Indian Ocean and the next dominant mode as Dipole mode.

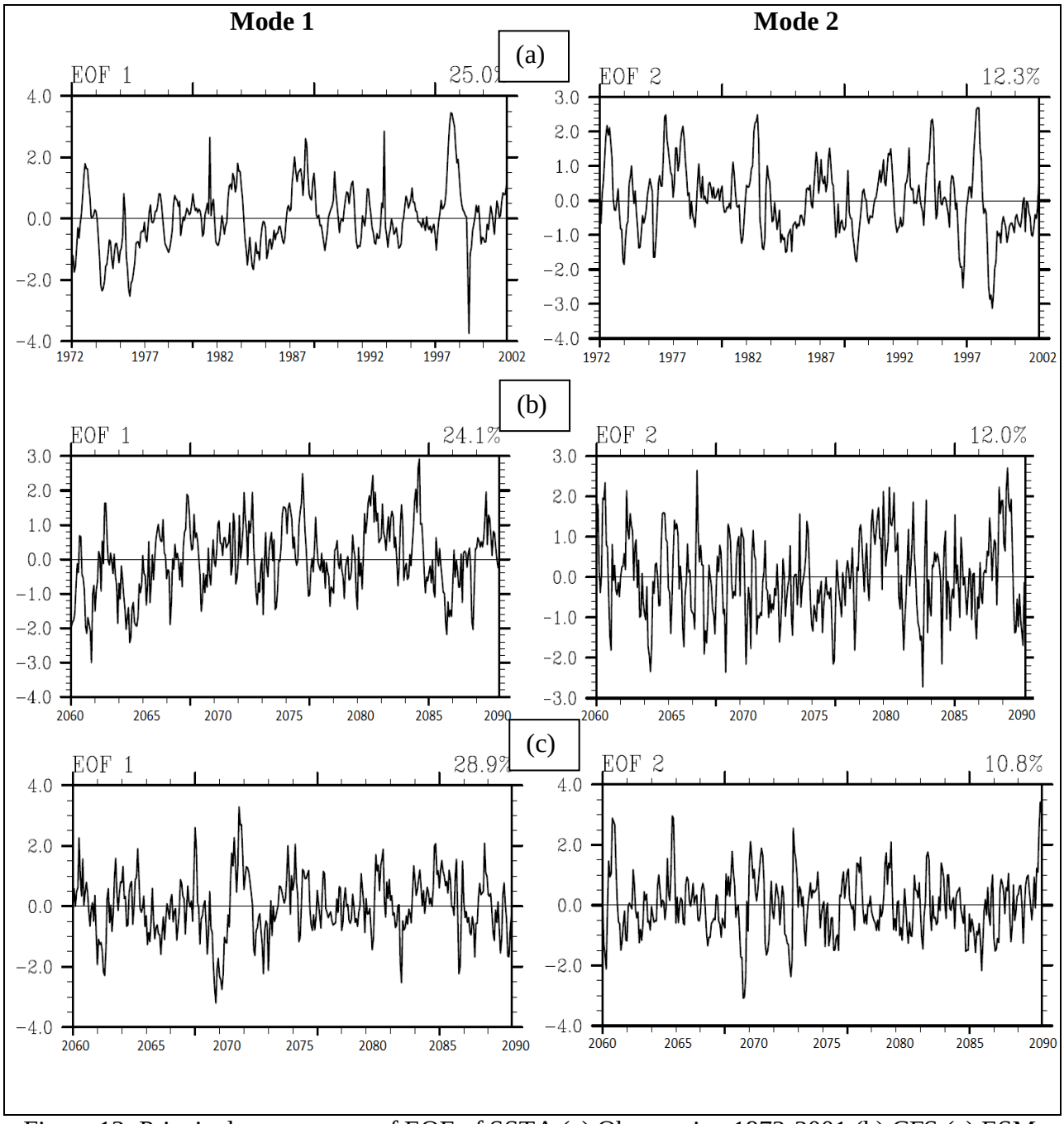


Figure 12: Principal components of EOF of SSTA (a) Observation 1972-2001 (b) CFS (c) ESM

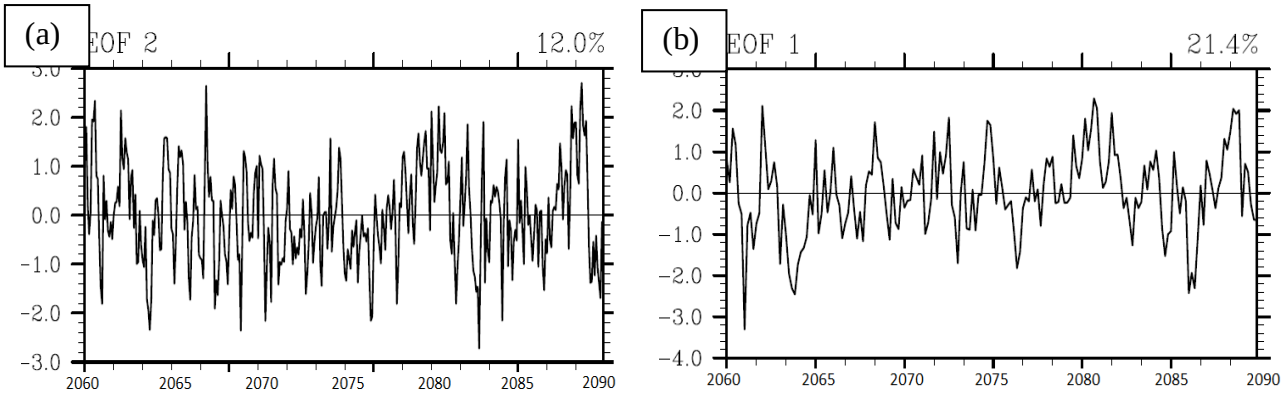


Figure 13: Time series for EOF SST, comparison to observe noise reduction (a) CFS- complete year (b) CFS- JJASON.

In order to account for the noisiness in the PC of EOF-2 of CFS, EOF of SST for only the IOD season, i.e. JJASON is done and the resulting PC are shown in Figure 13. Apparently the PC-2 has been smoothed out considerably giving an indication that the early IOD-like events in a year may be giving a noise in the inter-annual variability in the CFS. This is, to some extent, visible in the ESM as well.

It is rather intriguing to analyze whether the early events in the matrix for CFS are some intermittent signal or just noise. Since the time series in the JJASON EOF smoothed out such noises significantly, the spatial structure of the early events is looked upon. To elaborate the pattern a composite analysis was done, wherein the composite of all positive and negative events during JFMAM was done and the difference is plotted in order to enhance the signal (Fig 14). This composite map shows that the signal is a significantly mimicking an IOD structure.

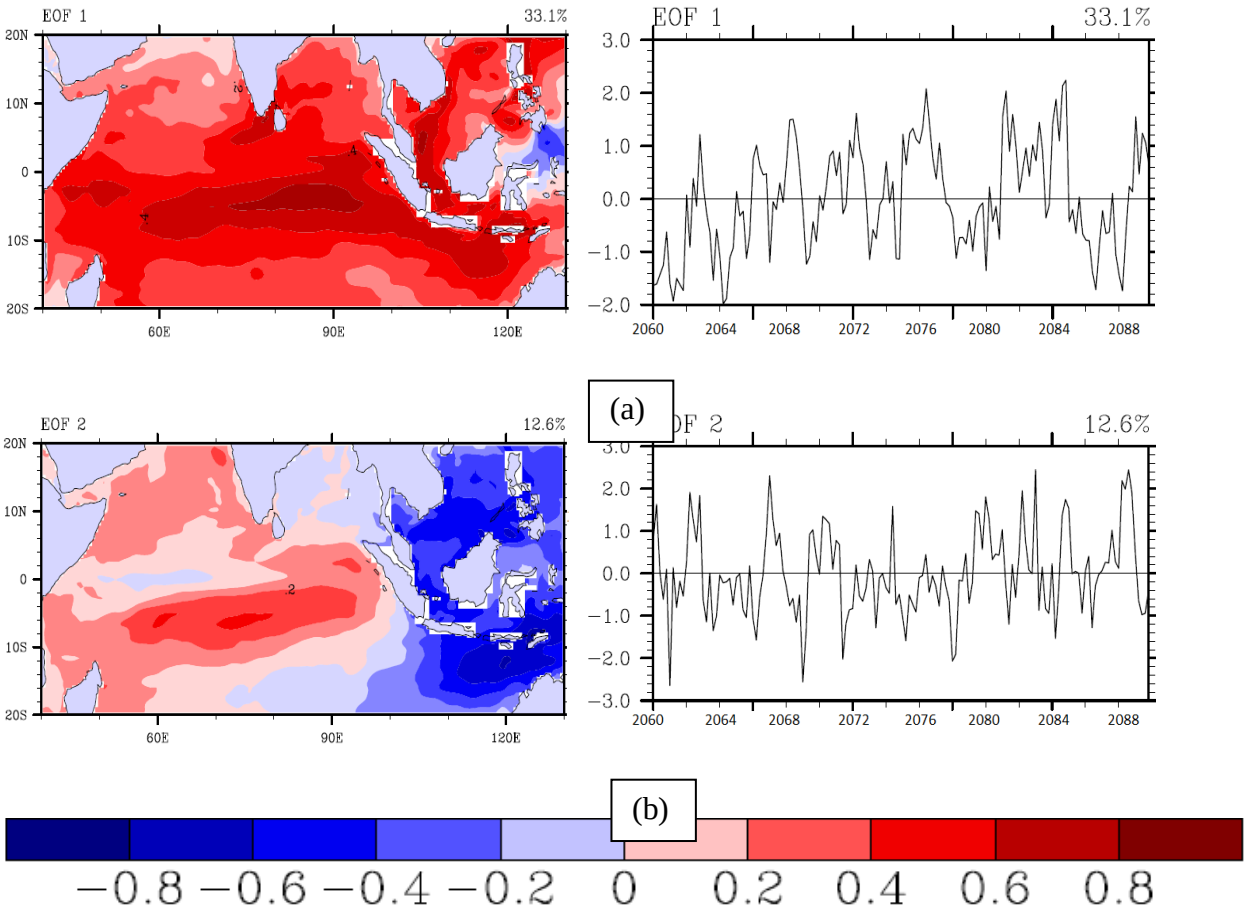


Figure 14: EOF of JFMAM, spatial map and principal components: (a) mode 1 (b) mode 2

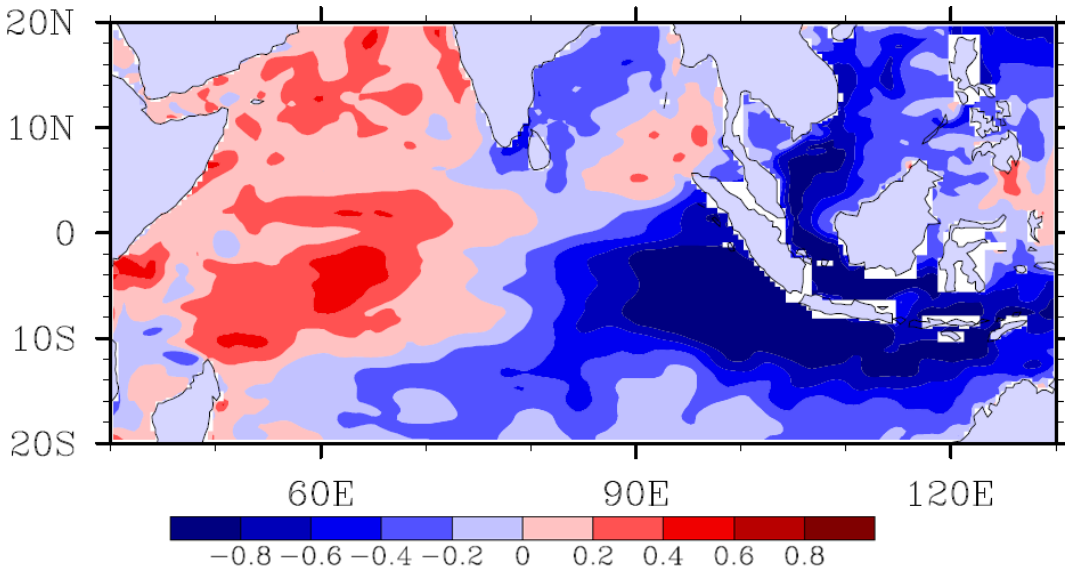


Figure 15: Composite of early 'IOD-like' events, (Positive – Negative).

## Chapter 4: Role of ocean biases in model IOD

IOD evolves in the equatorial ocean wave-guide as coupled ocean atmospheric phenomenon involving SST, sea surface winds, convection and precipitation. The oceanic subsurface also oscillates in similar fashion according to the wave dynamics. The oceanic responses during IOD are studied in previous studies (Vinayachandran et al., 2006, Rao et al., 2002).

From the above chapter it can be said that both the CFS and ESM models are simulating the Indian Ocean Dipole mode quite reasonably and realistically especially in the spatial structure. The spatial structure is very close to the observations. But the power spectrum of DMI of both the models has significant difference from the observations, especially in terms of both periodicity and amplitude. Also, the matrix showing the IOD indices shown in Fig 10 has significant differences between the models and observation. It appears that there exist 'spurious' IOD like signatures in the model in the early part of the year (i.e. during JFMAM).

In the previous chapter on validation of models, it was clear that even though the surface features are consistent with the observations, there were biases in the subsurface of the model. The warm biases (as clear from the temperature profile) may have a role in affecting the ocean dynamics, if thought as the subsurface and surface dynamics are linked via normal-mode theory (Gill, 1980). In this chapter we examine the role of subsurface ocean biases on the evolution of model IOD, and lights into the topic of 'spurious' IOD like early year phenomenon in the model and see whether they are related to the oceanic biases.

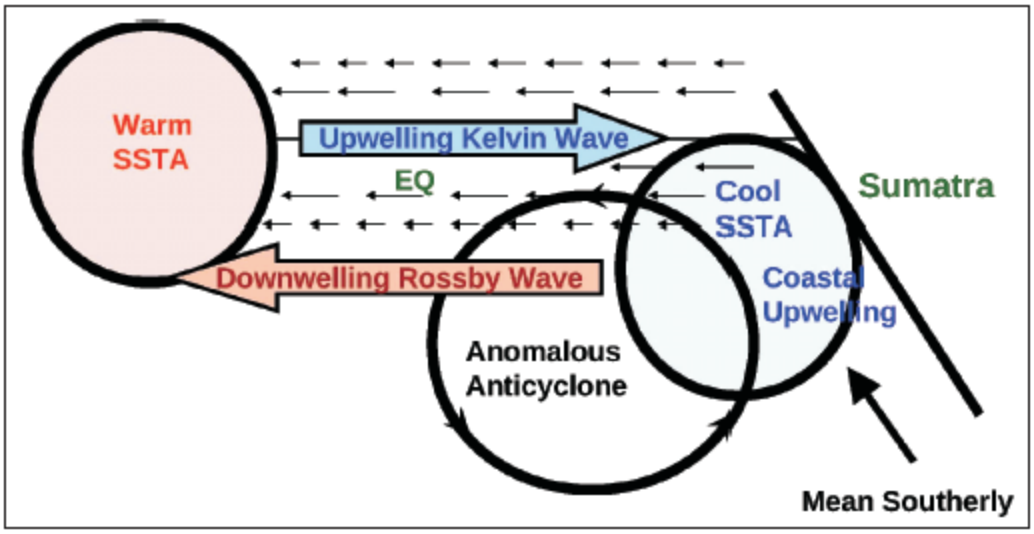


Figure 16: Schematic showing the coupled positive feedback in the Indian Ocean (Vinayachandran et al,2006)

Before proceeding further, we present here the feature of IOD as a coupled phenomenon. A positive feedback (Fig 16) exists between the SST and winds, which sustain the event long enough to be an important part of the variability for the entire basin.

A drop in SST in the SETIO implies a corresponding drop in cloud amount in situ. A decrease in atmospheric convection leads to the development of descending Rossby waves to the west (Gill 1980), resulting in an anomalous anticyclonic circulation to the west of decreased convection center. Since, winds along SETIO are southeasterly during the development phase of IOD, the anticyclonic circulation enhances wind speeds in the SETIO. The enhanced winds, in addition to driving coastal upwelling and vertical mixing, induce strong evaporative cooling of the sea surface, leading to more cooling of the SETIO (figure16). This positive feedback acts only during boreal summer, as mean winds along SETIO reverse in the fall (Vinayachandran et al. 2006).

The matrix, in Fig 10, which presents the evolution and decay of dipole mode, draws the attention towards the difference between the observation and model studies. It is seen that there are a considerable number of events taking place in the earlier part of the year, in both the models. These may not necessarily develop into seasonal IOD for the later part of year. The frequency of these events is higher in CFS as compare to ESM.

A fundamental variable in dynamics of stratified fluid flow that is able to connect the vertical structure of the ocean and its bias to the thermocline dynamics is the Brunt Vaisala frequency ($N^2$, also called buoyancy frequency). It quantifies the importance of stability and is the maximum frequency with which internal modes can oscillate. It is used as a measure of stratification or resistance to turbulence. In a continuously stratified fluid, the squared buoyancy frequency is

$$N^2 = -\frac{g}{\rho_0}\frac{d\rho}{dz}$$

Where g is acceleration due to gravity, and ρ is the density.

$N^2$ is plotted for the observation, CFS and ESM (Fig 17). $N^2$ generally goes higher around the thermocline region showing a sharp gradient in the buoyancy frequency at which the baroclinic modes are separated. The major peak in $N^2$ with depth shows the dominant first mode structure in the ocean dynamics. From the figure it is clear that the profile has a smooth curvature with depth for the observations, but in case of models it is not. There is a sharp gradient in ESM, visible quite clearly.

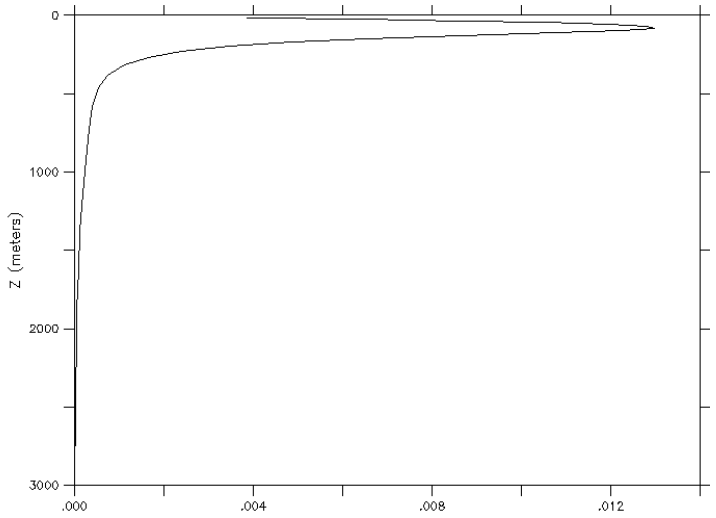


(a)Observation

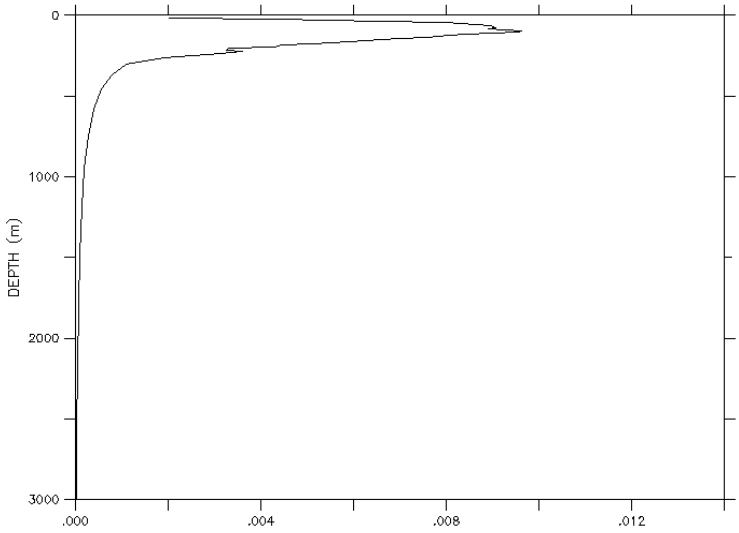


(b)CFS

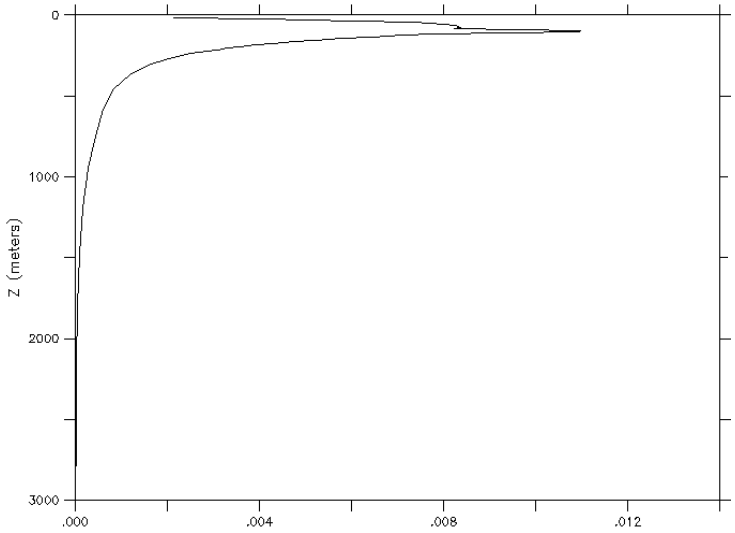


(c)ESM

Fig: 17: $N^2$ profile for (a) Observations, (b)CFS and (c) ESM

The fundamental difference in the $N^2$ structure in two models from the observations show that the normal-mode structure of the ocean within which the dominant baroclinic mode are set-up between the free-surface and ocean bottom have influence in the baroclinic dynamics of the system. This can be realized by The WKJB approximation, which defines a modified vertical co-ordinate, according to which the phase Φ varies linearly with z for slowly varying N (Gill, 1982).

$$\varphi = c^{-1} \int N \, dz$$

This transformation does not depend upon frequency, when hydrostatic approximation is made. Therefore for the normal modes, between rigid boundaries at z=0, -H, which change phase by integral multiple of π over the depth of fluid, and thus gives

$$c_n = \int_{-H}^{0} N \, dz / n\pi$$

where, n=1,2,3,… represents first, second, third etc. baroclinic speeds. Then for any given baroclinic mode 'n' $c=c_n$ gives the speed of that particular baroclinic mode with which the planetary waves disperses. Utilizing this theorem, we obtained the speed for the first baroclinic mode for internal gravity waves in CFS and ESM and compared it with those deduced from the observations.

The first baroclinic speed for the observation comes to be nearly ~3m/s in the tropical Indian Ocean (figure not shown). The bias of the same in CFS and ESM was calculated. There is a positive bias in the baroclinic speed in both the models. (Fig 18) The white areas show the island topography and mid-oceanic ridges in the Indian Ocean where the vertical integration of $N^2$ is not possible.

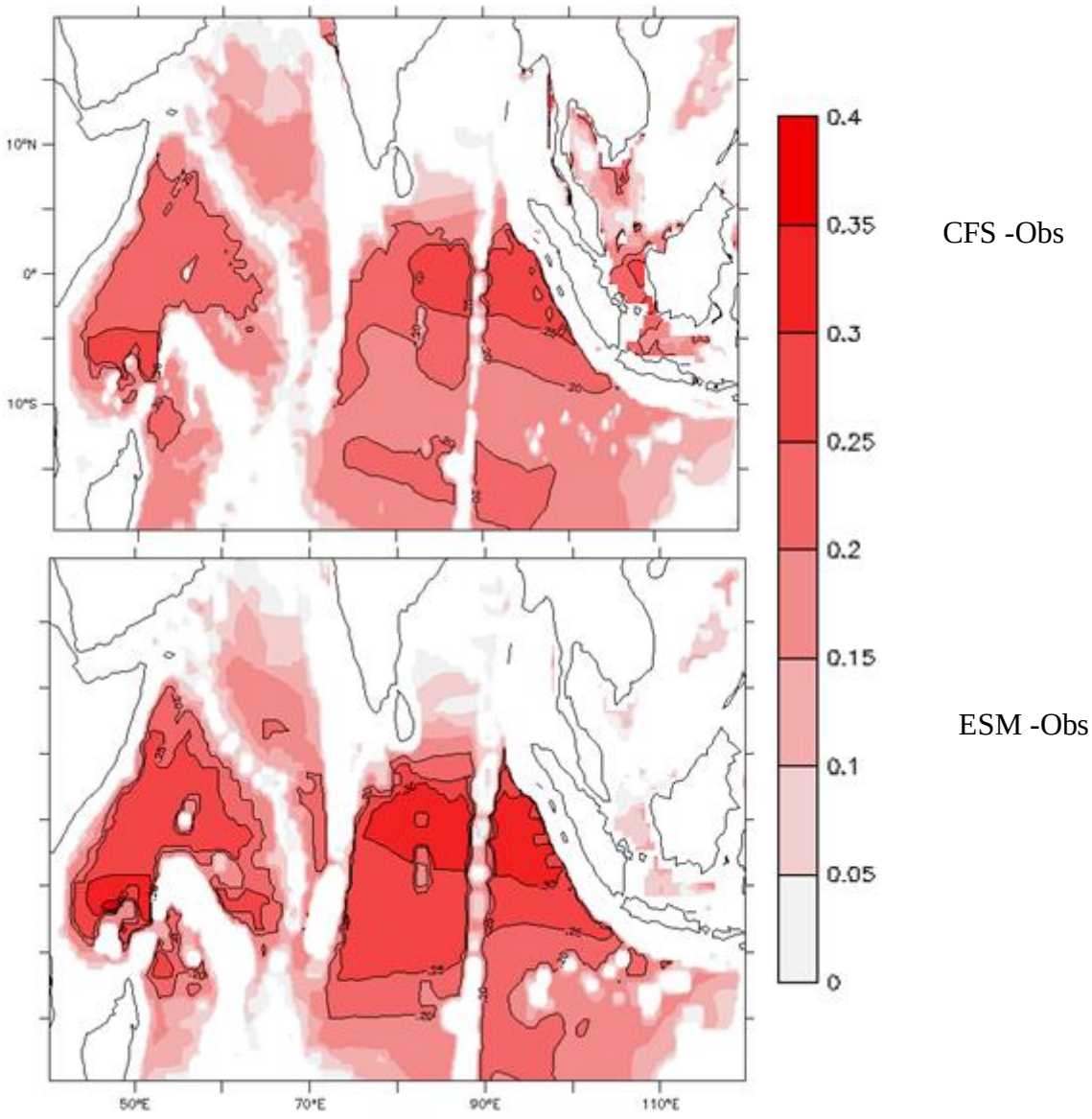


Fig 18: The bias of first mode baroclinic speed (a) CFS (b) ESM. Units in m/sec.

This bias in baroclinic speed shows that the waves are travelling at a faster pace in the model ocean than that in observation. It is around an extra of 0.25 m/s in CFS and around 0.3 m/s in ESM. A bias of 0.3 m/s means approximately 10% faster wave speed. The bias is higher in ESM. The speed of baroclinic mode is equal to the speed of Kelvin wave at the equator, and the speed of Rossby Wave is $1/3^{rd}$ of the Kelvin wave speed in the non-dispersive case. So if the bias is 0.3 m/s for mode-1, it induces an extra speed of 0.1 $ms^{-1}$ for the Rossby wave. In that case, if a

time period of 2 months are considered, distance = speed x time, which translates into 0.1 x 60 x 86400 ~ 500 km i.e. 5° longitudes covered extra in just two month. We hypothesis that such 'faster dispersion' can have effect on growth the spurious IOD like features in the models which we will prove by utilizing an ocean-only model experiment in the next sub-section.

A notable point is that a bias in the stratification gives rise to wrong $N^2$ profile and thus an incorrect baroclinic speed. So it can be said that the bias has a significant role on the characteristics of phenomenon such as IOD. To verify the role of bias in stratification on resulting IODs in the model, several experiments were done on a 3-1/2 layer reduced gravity model, forced with different sets of winds and initialized with different sets of background stratifications.

### 4.1 Model Experiment

#### 4.1.1. Reduced gravity ocean model

In a three-layer approximation of the ocean, the gravity waves can exist on either the interface at the top of the upper fluid, or on the interface between the two fluids. The waves on the top and on the interface are not independent. Instead, they are locked together in two or more possible modes. Barotropic mode is in which the two surfaces move in phase with one another as shown in Figure 19.

In the baroclinic phase, the two waves have opposite phases. The literal meaning of 'barotropic' is that pressure is constant on surfaces of constant density, and hence is constant on interface. 'Baroclinic' means pressure is not constant on surfaces of constant density.

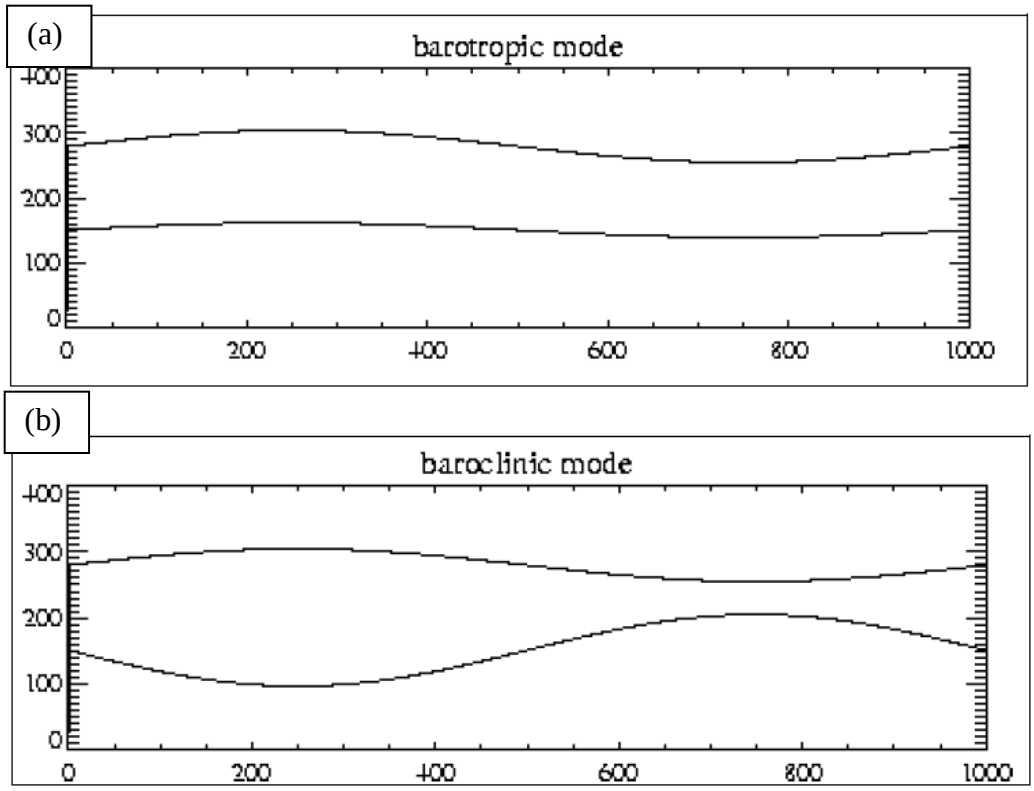

Fig 19: (a) Phase of surfaces in barotropic mode (b) Phase of surfaces in baroclinic mode

Some model experiments were done in order to investigate the role of stratification and wind anomalies in the CFS and ESM in generating 'spurious' IOD like features. We use a representation of the ocean as a layered model. This is a reduced gravity hydrodynamic model with N-full layers under motion with a 1/2 abyssal layer at rest (Valsala 2008). Thus the barotropic mode is filtered out in the model by setting the bottom layer stagnant and limiting the gravity to operate under the density differences between the layers (i.e. reduced gravity). The model has a realistic coastal boundary and fully non-linear dynamics (i.e. the variable layer thickness and velocity interact each other). The model domain contains the tropical Indian Ocean with closed boundaries on all sides. The boundary at the southern Indian Ocean gives rise to reflected waves near the boundary, but our equatorial domain is. So there is no harm with the boundary on the time scale we are considering.

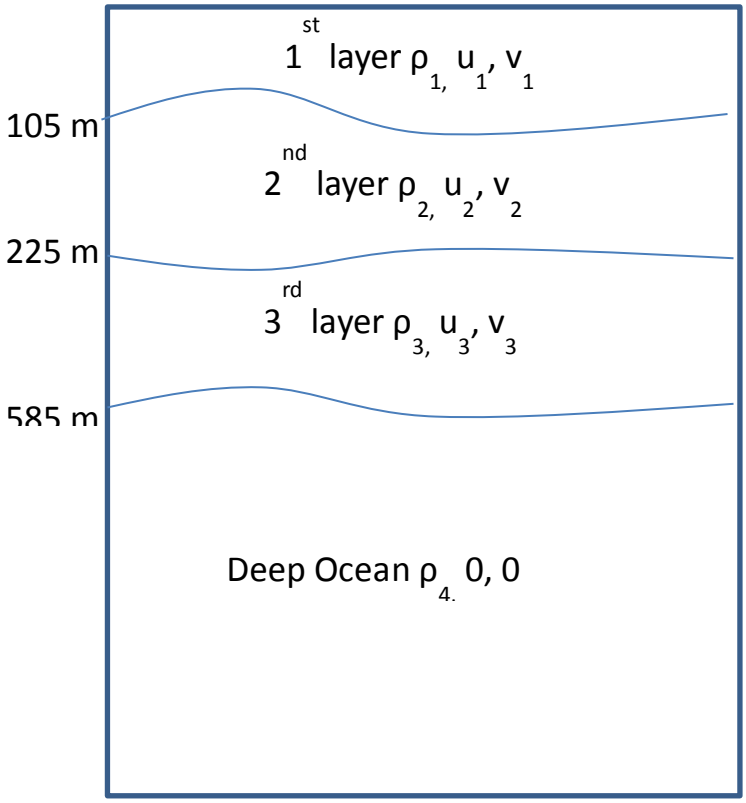


Fig 20: The 3-1/2 reduced gravity model.

The model is then configured with 3-1/2 layer structures. The thicknesses of the first, second and third layers were chosen as 105 m, 225 m and 585 m respectively. The choice of these layer thicknesses and corresponding depth averaged density values is determined by looking at observations in the Indian Ocean.

### 4.1.2 Forcing

We force the simple layered model with CFCv2 monthly wind anomalies, with CFCv2 stratification and also with observed stratification in first two cases. For a comparison, we also forced the above two cases with NCEP/NCAR re-analysis wind anomalies. Both the experiments

were run for 30 years. Note that the simple model was initialized at rest and only wind anomalies are used to force them, therefore there is no mean circulation in the model. The logic of this experiment is to identify, for a given stratification and wind anomalies, what is the time-space scale evolution of equatorial waves, which is also playing a key role in the real IOD dynamics.

We took the CFS wind anomalies and density structure for the model domain; basin averaged over 20°S-20°N, 30°E-110°E. Similarly, the same is done for the observations, with NCEP winds and SODA stratification for the same basin average. Now we have 4 cases for all combinations possible.

Case 1: CFS wind anomalies over CFS stratification.

Case 2: CFS wind anomalies over SODA stratification.

Case 3: NCEP wind anomalies over CFS stratification.

Case 4: NCEP wind anomalies over SODA stratification.

The model is allowed to run and output were sampled every 15 days, that is twice a month.

In these experiments, the layers of the simple model undergo dynamical changes according to first three baroclinic modes (because of 3&1/2 layer system). Case-1 will gives the IOD type of thermocline movement in the model for the given CFCv2 wind anomalies. Case-2 will give the similar evolution but identifies the effects of CFSv2 stratification on the wave dispersion. Therefore the difference between Case-1 and Case-2 will give the effect of bias in stratification on wave dispersion for given CFSv2. Similarly difference between Case-3 and Case-4 will give the effect of bias in the stratification on wave dispersion for given NCEP winds.

4.1.2 **Model solutions**

EOF analysis is performed on the sea surface height (η) of all the cases. Sea surface height is a proxy for the thermocline movement and also the sea surface temperatures. Also, it shows the response of net effect of all the baroclinic modes. If we just take the first layer, it may represent only the mode-1, but the SSH has all the possible modes combined together.

At first we have done the EOF of η for all the four cases. On analyzing the EOF spatial patterns of individual cases (Fig 21) it seems that the spatial pattern is quite consistent with the IOD positive phase. However there are considerable differences in the principal components of each of these cases. The high frequency 'noise' in the PC of Case-1, which is purely CFSv2 based experiment, was larger compared to Case-4, which is purely based on observational data based experiment. This indicates that, even though the spatial loading of EOFs looks similar, there exist an intermittent positive and negative 'wiggling' to the EOF-1, especially in cases forced with CFS winds and stratification. At this stage one can anticipate this oscillatory nature may be coming from the CFSv2 wind anomalies and/or from the bias in the stratification. Following analysis was done in order to separate these two effects.

Case-1 shows the pure model case wherein the CFS winds and CFS stratification are used, and Case-4 is the pure observation case, wherein NCEP winds on SODA stratification are used. Even though the spatial map looks perfectly similar, all the time series are entirely different. The PC-1 of model is too noisy compared to that of the observations, which is rather smoothed out. It should not be missed out that when model winds are used, the time series is very noisy (Case-1 and 2), however with observed winds case, the stratification brings in a noise (Case-3),

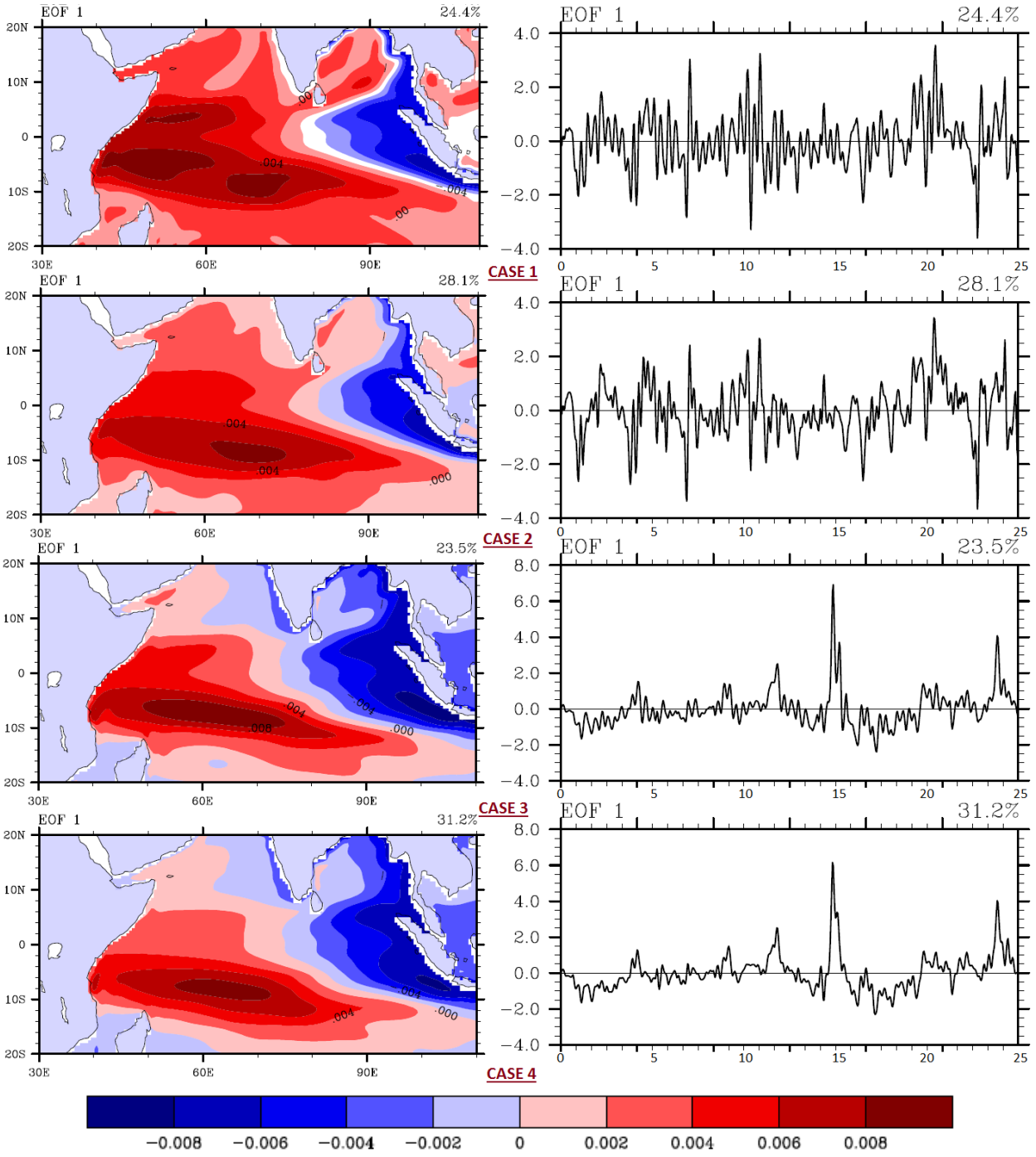


Fig 21: The spatial plots and principal components of EOF performed on Sea surface Height obtained from all the cases. The spatial plots are very consistent, but the time series vary significantly.

by model winds. So, it can be said that the model winds are noisy, and stratification adds to it.

For the purpose of analysis, we take the differences of η between Case-1 and Case-2, and have done the EOF analysis on that. This will give us the effect of different stratification when forced by same CFS wind anomaly. The EOF analysis of Case1-Case2 (Fig 22) shows that the spatial pattern is coherent with the spatial plot of composite of the early 'IOD-like 'events (Fig 15). The warming in the west and cooling in east in the composite is similar to that the EOF of Case-1-Case-2. This is rather curious to note that just because of stratification bias a 'spurious' IOD look-a-like phenomenon is possible to be established in the model.

The time series of this EOF has very high frequency noise. A power spectrum analysis of the time series results with the dominant peak in 4-5 months (Fig 23). Since the data has 2 points for each month this corresponds to, $8^{th}$-$10^{th}$ time levels in the power spectrum. By cross-examining the PC-1 of Case-1 and Case-1-Case-2 we may deduce that the model stratification add to the noise and produces high frequency oscillations.

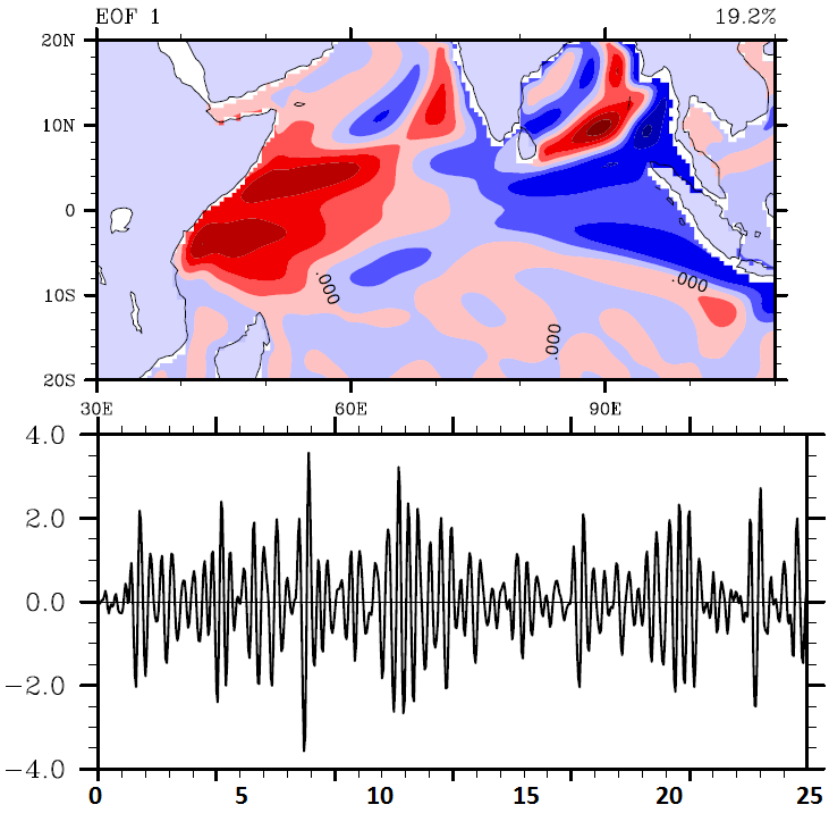


Fig 22: The spatial plot and PC for η [Case-1- Case-2]

It is rather intriguing to consider that the EOF-s of Case-1-Case-2 resulted a spatial structure almost similar to what is seen in the composite maps of SST anomalies in the 'spurious' IOD like events in the early part of the year in the CFS and ESM. This is rather interesting because, one may bring out a conclusion that, just by the differences in the stratification, which adds as some 'extra' or 'less' speed to the baroclinic system can bring oscillatory nature to the dispersion of waves. This is rather though-provoking because the size of the equatorial Indian ocean is rather small (1/3$^{rd}$ of the Pacific) and such 'fast' dispersion of the equatorial waves cannot be neglected.

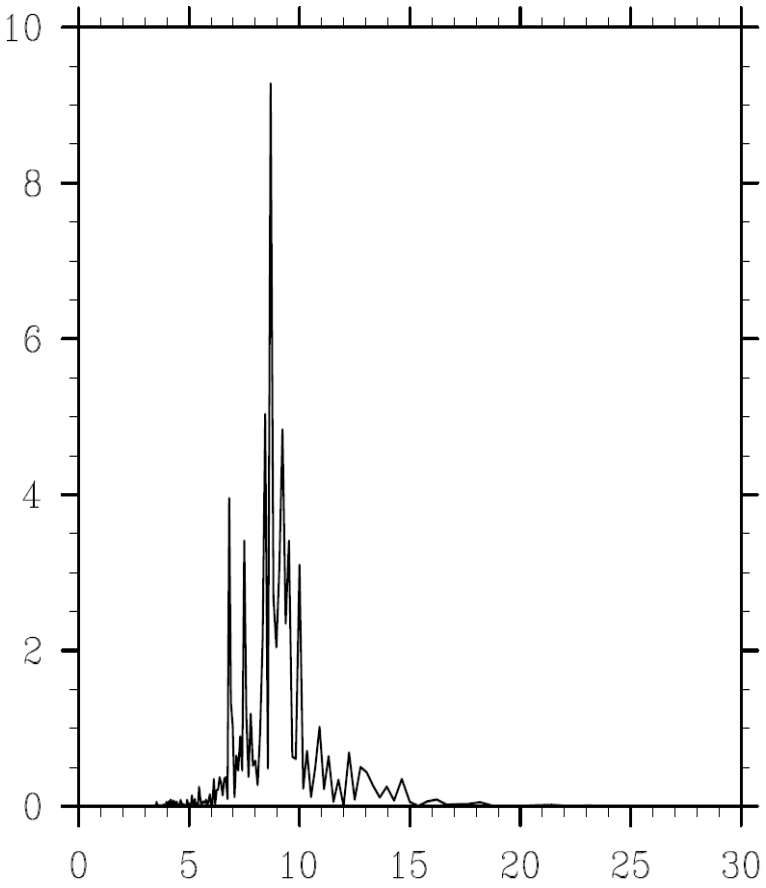


Fig 23: Power Spectrum of PC time-series for η [Case1-Case2]

Similar analysis is done for SSH (Case-3-Case-4), which shows the effect of difference in stratification when it is forced by NCEP wind anomaly. This has been done in order to isolate the effect of stratification alone in generating the noise. In this case, the wind is observed (re-analysis) therefore difference between Case-3 and Case-4 solely reflects the effect of bias in stratification on equatorial wave dispersion.

In this case as well the spatial plot resembles the composite map for early IOD-'like' events and the time series is very noisy. A power spectrum of the PC looks similar to Fig 23.

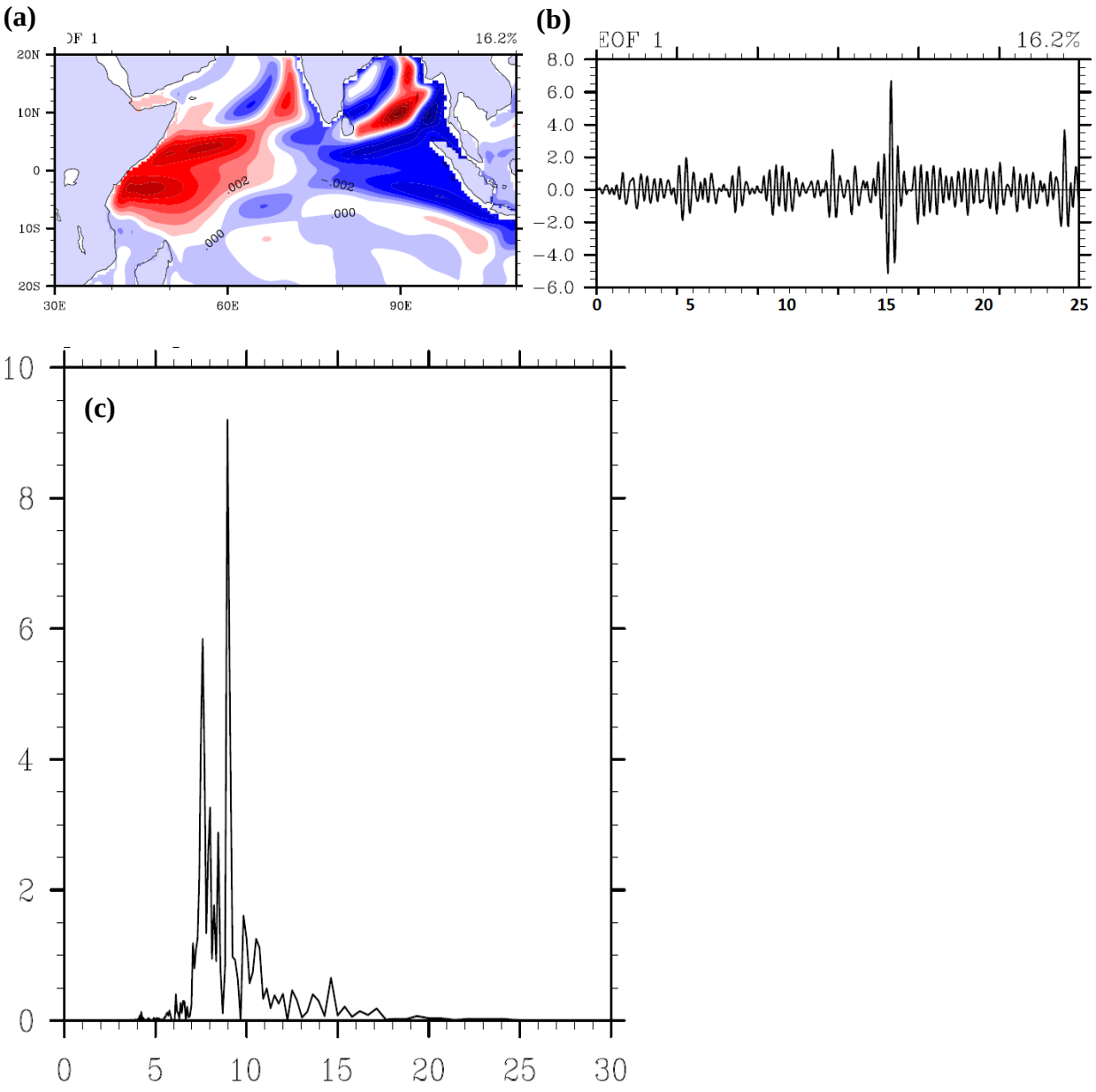


Fig 24: (a) Spatial plot for EOF-1 of η[Case-3 – Case-4], (b) PC1 (c) Power Spectrum for PC1.

Though the two power spectrum plots look similar, and show almost the same periodicity, we noted that the peak for η (i.e. PC-1 power spectrum of Case1-Case2) has shifted slightly to the left that of η (i.e. PC-1 powers spectrum of Case 3-Case 4). Moreover, the earlier has higher amplitude in power than the later. This shows that high frequencies get incorporated when CFS winds are used and bias in the stratification adds to the noise in wave dispersion.

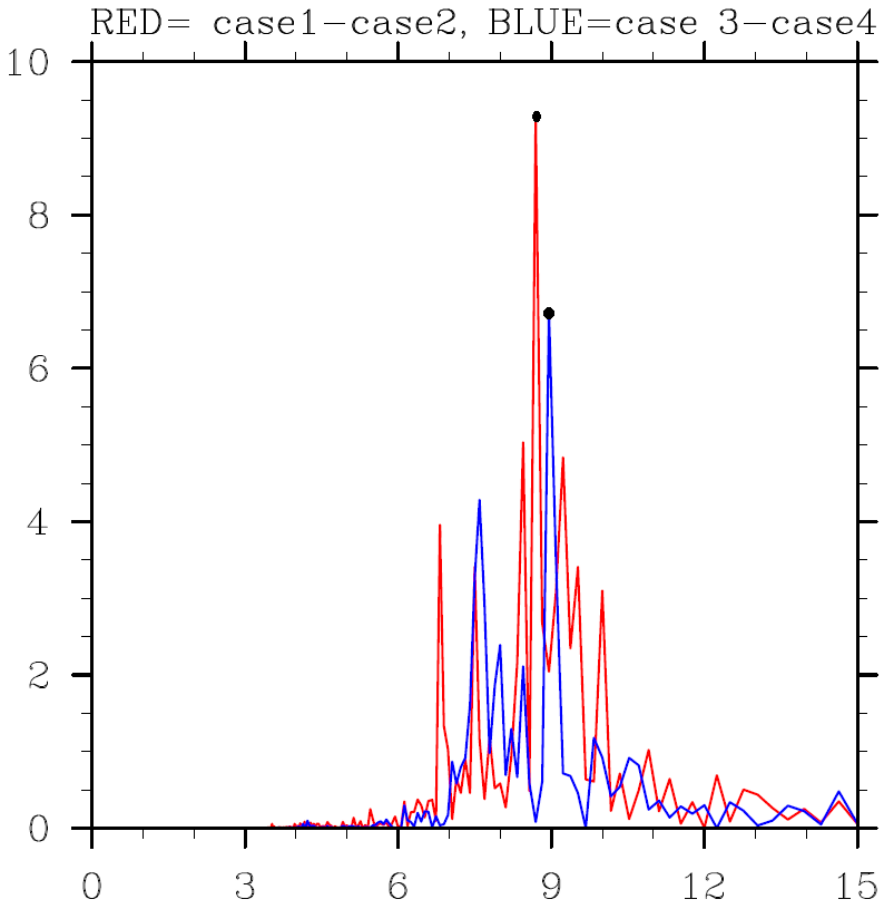

Fig 25: The power-spectrum of PC-1 for η[Case1-Case2] in red, η[Case 3-Case4] in blue

Based on the above results and in order to identify the cause of 'such' spurious oscillation by way of biases in the ocean structure, we put forward a hypothesis, what we name as 'short term intensification of feedback'. For instance, suppose there is a wind perturbation in the equatorial ocean. This leads to an east-west separation of SST anomalies via Kelvin-Rossby wave dispersions. This enhances the wind if the SST anomalies are in favorable direction and the coupled system grows as in Bjerkness feedback (Bjerkness, 1969). Whereas, if there is a faster dispersion of equatorial waves, as suggested by the baroclinic speed bias, the separation of SST in east-west direction takes place relatively faster than usual. Once it separates, it may cause the winds to diverge from the cold center, and converge into the warmer center, thus the winds

become stronger. However the faster separation of east-west anomalies tends to reduce the further growth of wind and the system may not be growing into a full IOD. Moreover, in the model such 'spurious' events are occurring in the early part of the year where the absence of preconditioning, the monsoon winds and the heat source, the IODs of that season may not grow quickly.

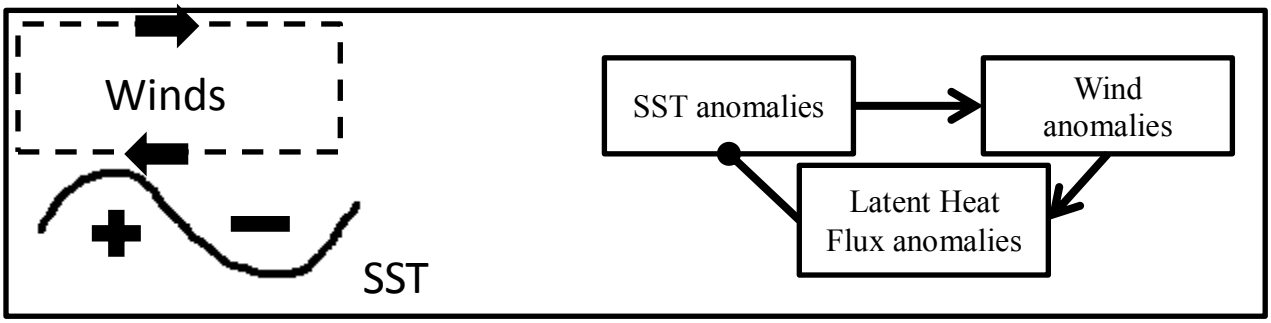


Fig 26: The possible setup for the development of short-term intensification of feedback and leading to a negative feedback

on the above hypothesis, we have formed an analytical frame work for the 'short-term intensification of feedback', with following two equations of coupled ocean-atmosphere system.

The equation-1 shows the growth or decay of equatorial thermocline gradient due to 'bias' in the baroclinic speed (i.e. $\Delta c$) and wind velocity ($\tau_x$). The equation-2 shows the growth of wind due to the resultant thermocline gradient. $\mu_1$ is the coupling coefficient, $\mu_2$ stands for the reduced-gravity of a two-layer atmosphere and $\alpha$ stands for a scaling factor which translates the thermocline gradient into atmospheric geopotential gradient. We assume the coupling coefficients $\mu_1$ as negative because the model solutions show a net negative feedback (see below). $\mu_2$ is considered as positive. $\mu_2\alpha$ collectively chosen an on the order of $10^{-6}$.

Initially the wind was assumed as an equatorial wind-perturbation at a constant value, and its growth or decay is set to zero. With these two systems of equations and two initial conditions, we attain a general solution of $\tau_x$ as a cosine function with frequency equal to $\sqrt{\mu_1\mu_2\alpha\Delta c}$. The equations and their solutions are given below.

$$\frac{\partial\left[\frac{\partial h_o}{\partial x}\right]}{\partial t} = \mu_1 . \Delta c . \tau_x \qquad (1)$$

$$\frac{\partial \tau_x}{\partial t} = \alpha\mu_2 \frac{\partial h_o}{\partial x} \qquad (2)$$

$\tau_x = \text{Zonal Wind}, \quad \frac{\partial h}{\partial x} = \text{thermocline gradient}, \quad \alpha, \mu_1, \text{ and } \mu_2 = \text{constants}$

Boundary conditions; $\tau_x = 1 \text{ at } t = 0 ; \frac{\partial \tau_x}{\partial t} = 0 \text{ at } t = 0$

When simplified equatinos (1) and (2) give us :

$$\frac{\partial^2 \tau_x}{\partial t^2} + \mu_1\mu_2\alpha\Delta c\tau_x = 0$$

This is a second order homogeneous differential equation.

The characteristic equations is : $m^2 + \mu_1\mu_2\alpha\Delta c = 0$

The general solution of the characteristic equation $r^2 + ar + b = 0$ is as follows:

- Real and distinct roots: α, β

If $a^2 > 4b$, in which case the characteristic equation has distinct real roots, the general solution of the equation is $Ae^{\alpha t} + Be^{\beta t,}$

- Real and equal roots: - α/2

If $a^2 = 4b$, in which case the characteristic equation has a single root, the general solution of the equation is $(A + Bt)e^{\alpha t}$ .

- Complex roots: , $m_1 = \alpha+i\beta$ , $m_2 = \alpha-i\beta$

If $a^2 < 4b$, in which case the characteristic equation has complex roots, the general solution of the equation is $e^{\alpha t}(A\cos(\beta t) + B\sin(\beta t))$.

A, B are constants, which can be calculated from initial conditions which are 1 and 0, respectively.

In our case, the roots are complex because of negative sign of $\mu_1$ so applying the initial conditions, we get their general solution of the form:

$\tau_x = \cos\sqrt{\mu_1\mu_2\Delta c}\,t$ for $\mu_1 < 0$ and $\mu_2 > 0$ .

Now, using the scale analysis, if $\tau_x$ = 1 m/s; L = 50° = 5 x $10^6$ m; $\alpha$ = (30-days)$^{-1}$

$\mu_1 = \frac{1}{U}.\frac{1}{L}$ = 0.2 x $10^{-6}$; $\mu_2 = \tau_x$ =1;

$1/\sqrt{\mu_1\mu_2\Delta c}$ = period (T) ~ 3-4 months

It appears that the periodicity is roughly 3-4 months which is quite similar to the power of PC-1 in our Case-1-Case-2 experiment described above. This means that the negative coupling (see below) causes the solution to be stable and oscillatory in time. Note that this solution turns to a stable and non-oscillatory solution if the bias in baroclinic speed (i.e. $\Delta c$) is zero, in which case the cosine functions equal to one. In the case of model solutions of CFS and ESM, such spurious mode gives an oscillatory noise in the principle components of EOF-1 and 2.

A reasonable argument that such 'spurious' IOD modes are not growing, was explained in terms of SST-moisture negative feedback mechanism. Imagine the wind is initially perturbing the equatorial ocean; the east-west separation of SST is achieved. In our case, the bias in the dispersion of waves makes this separation faster than in reality. The corresponding increase in

wind which is blowing into the direction of positive SSTs, evaporate the ocean and can cool the SST development. This can leads to a negative feedback.

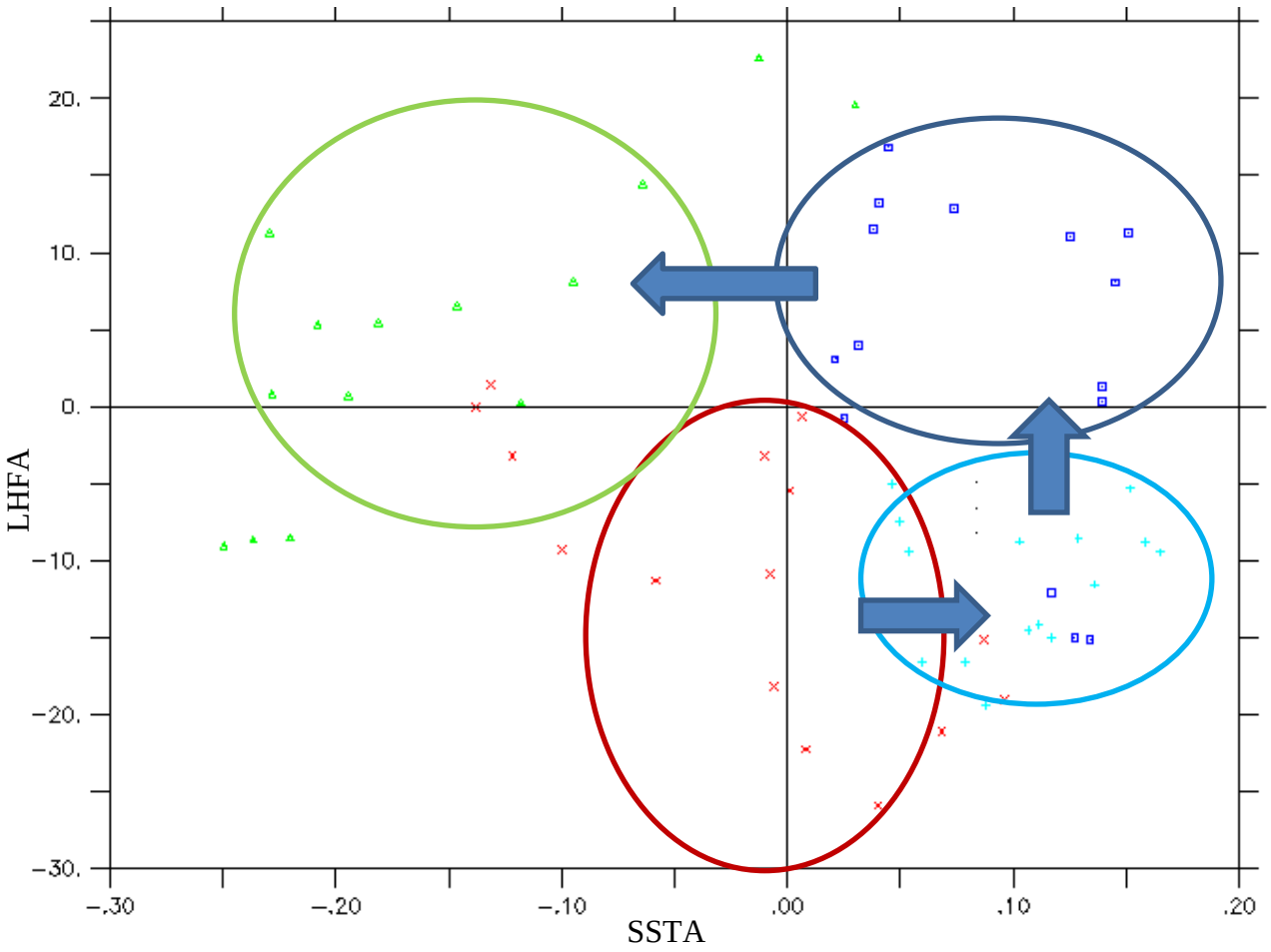


Fig 27: The composite for LHFA, for 60 days from the start of a positive event. Red: 1-15day, Light Blue: 16-30 day, Dark Blue: 31-45day, Green: 46-60day.

In order to provide a proof for this mechanism, we have examined the SST and latent heat flux anomalies (LHF) on the first 60-days of such 'spurious' IODs in the earlier part of the year in the CFS model. The composite of 60-day evolution of such positive events are plotted as SST anomalies versus the LHF anomalies. Fig 27 shows the scatter plot of SST and LHF anomalies averaged over $50^0$E-$60^0$E and 2°-$8^0$S (west box) and $60^0$E-$90^0$E and $5^0$S-$5^0$N

(equatorial box), respectively. In the early stages, the SST starts to warm up to 30 days. Up until this time, the LHF anomalies are negative meaning that there is no cooling. But from day 31 to 45 the LHF anomalies are positive which mean that the ocean is cooling. From day 31 to 60 the SST cools and this might 'kill' the wind anomalies. This may be a reason such 'spurious' modes are not growing in time. This situation matches with the analytical solution described above. However, further studies are required to ascertain this. Also, the role of pre-conditioning of monsoonal heat source and winds are not considered in our simple analytical model.

## Chapter 5: Relationship with monsoon

The Indian summer monsoon rainfall (ISMR) occurring during June-September plays a crucial role on both agriculture and economy of the Indian subcontinent (Parthasarthy et al, 1994). Whenever an El-Niño occurs in the Pacific Ocean, it is observed that there is anomalous decrease in the ISMR that season. This is due to the shift in the Walker Circulation. However, it is observed that when a positive IOD event occurs in Indian Ocean co-occurring with the El-Niño in the PO, the IOD seems to pull back the monsoon, and ISMR is normal or above normal. Hence, it is important to look at this IOD-ISMR relationship.

In this study, we mainly focused on the evolution of IOD in two models, CFSv2 and ESM and done a validation by comparing with the observations. Further, we also investigated on some 'spurious' IOD like features in the early part of the year in the CFSv2 and ESM, the reason of which we mainly associated to the bias in the vertical structure of the tropical Indian ocean that is resolved in the model. Upon such examinations, we further extended our study to see how well the IOD correlates with the ISMR in the model. This again serves as a validation of CFSv2 and ESM on climate change simulations.

The correlation map was constructed for the DMI-ISMR relationship at zero-lag from the observations (Fig 27). It is seen that the correlation is rather weak over the entire land region, and has a polarity in the ocean with positive correlation in the west, and negative in the east as explored in the previous studies(Ashok and Saji 2007). The same map when constructed for the models gives a very noisy picture, and is interpreted as a negative correlation in case of CFS, and weak correlation in case of ESM.

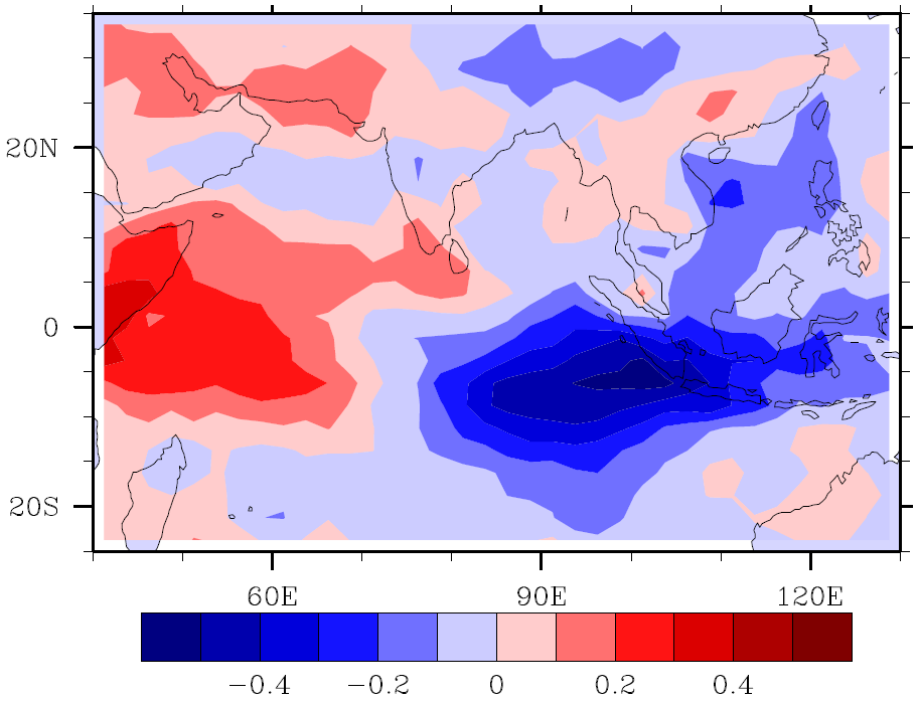

Fig 27: The correlation at lag 0 between DMI and Precipitation in JJAS in observation.

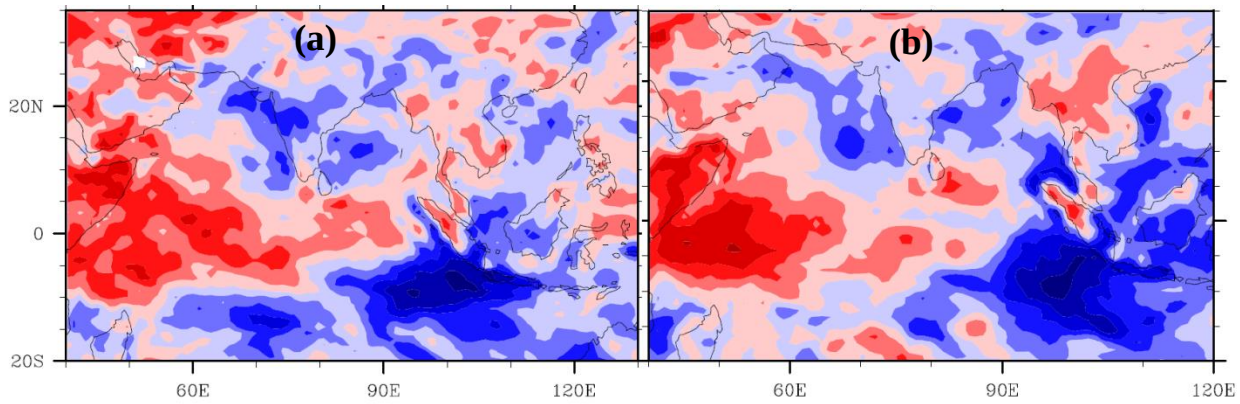

Fig 28: The correlation between DMI and precipitation for (a) CFS and (b) ESM

However, when the correlation was done on monthly scale, it is observed that the correlation is positive only for the month of July and August for the observations, but CFS in unable to capture this feature. In case of ESM, there is positive correlation only in the month of July in the form of a horizontal band spread latitudinal to the north of equator.

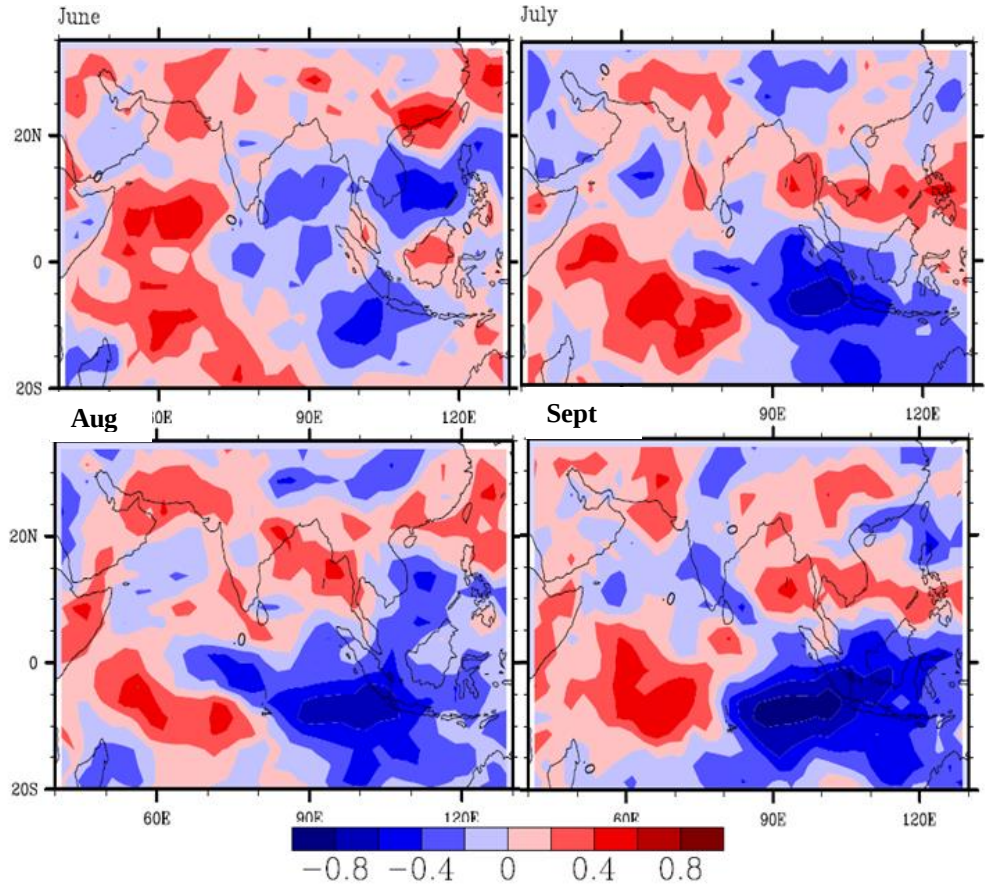


Fig 29: Month-wise correlations of IOD and ISMR for observations

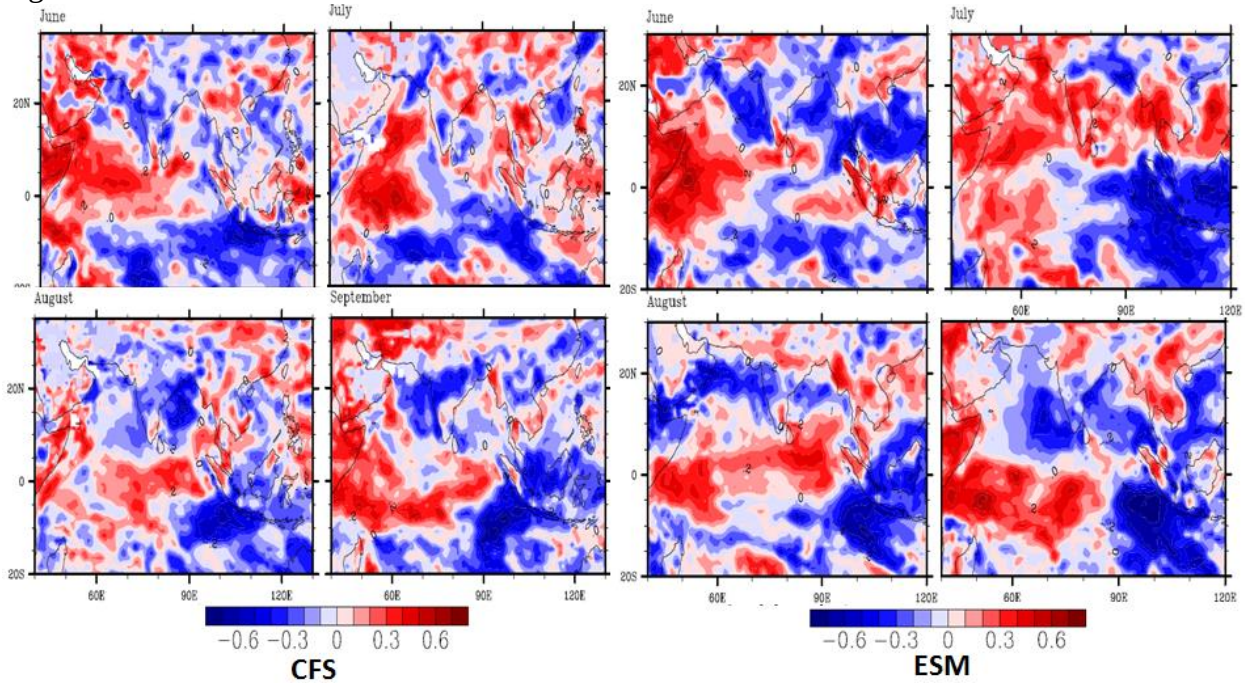


Fig 30: Same as above but for CFS and ESM.

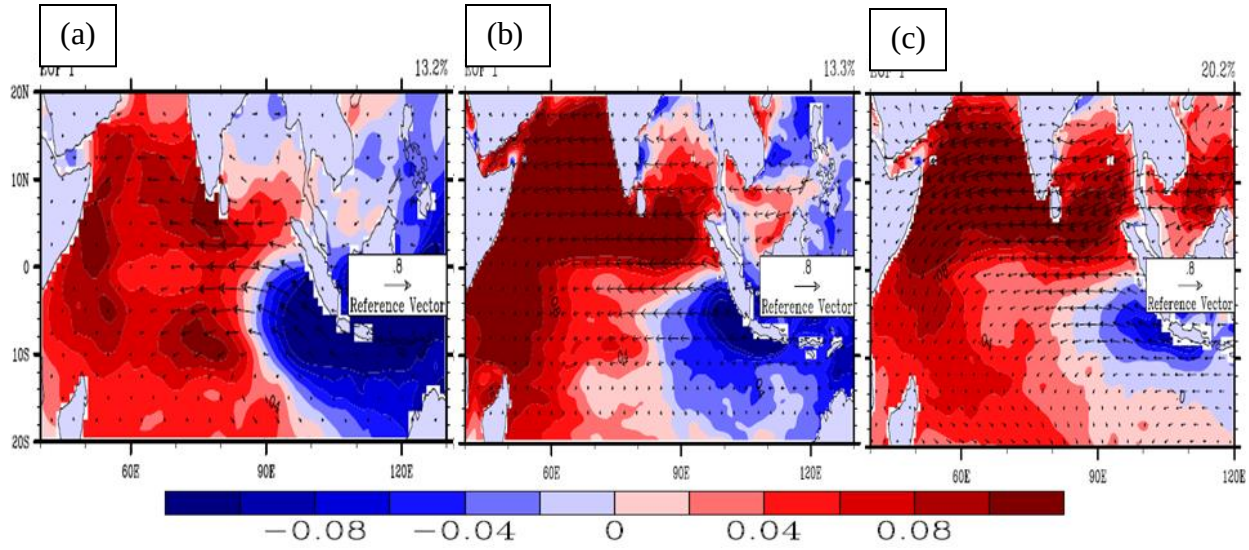


Fig 31: Multivariate EOF between SST and Surface winds for JJAS in (a) Observations (b) CFS (c) ESM.

The IOD affects the circulation over the Indian subcontinent, and can affect the monsoon. So, a coupled EOF analysis was done to see how the SST and winds couple and move together in their most dominant mode of variability. The observations show a dipole mode with cooling in the East Indian Ocean and warming in the west, the winds move from the colder region to warmer region. However these winds do not seem to move towards land, and grow very weak as we move away from the equatorial region. In CFS, the winds are strongly in the zonal direction, even the alongshore winds near Sumatra and Java are zonal. In ESM, the winds are zonal, but seem to turn at the west coast, and also near Java and Sumatra Island.

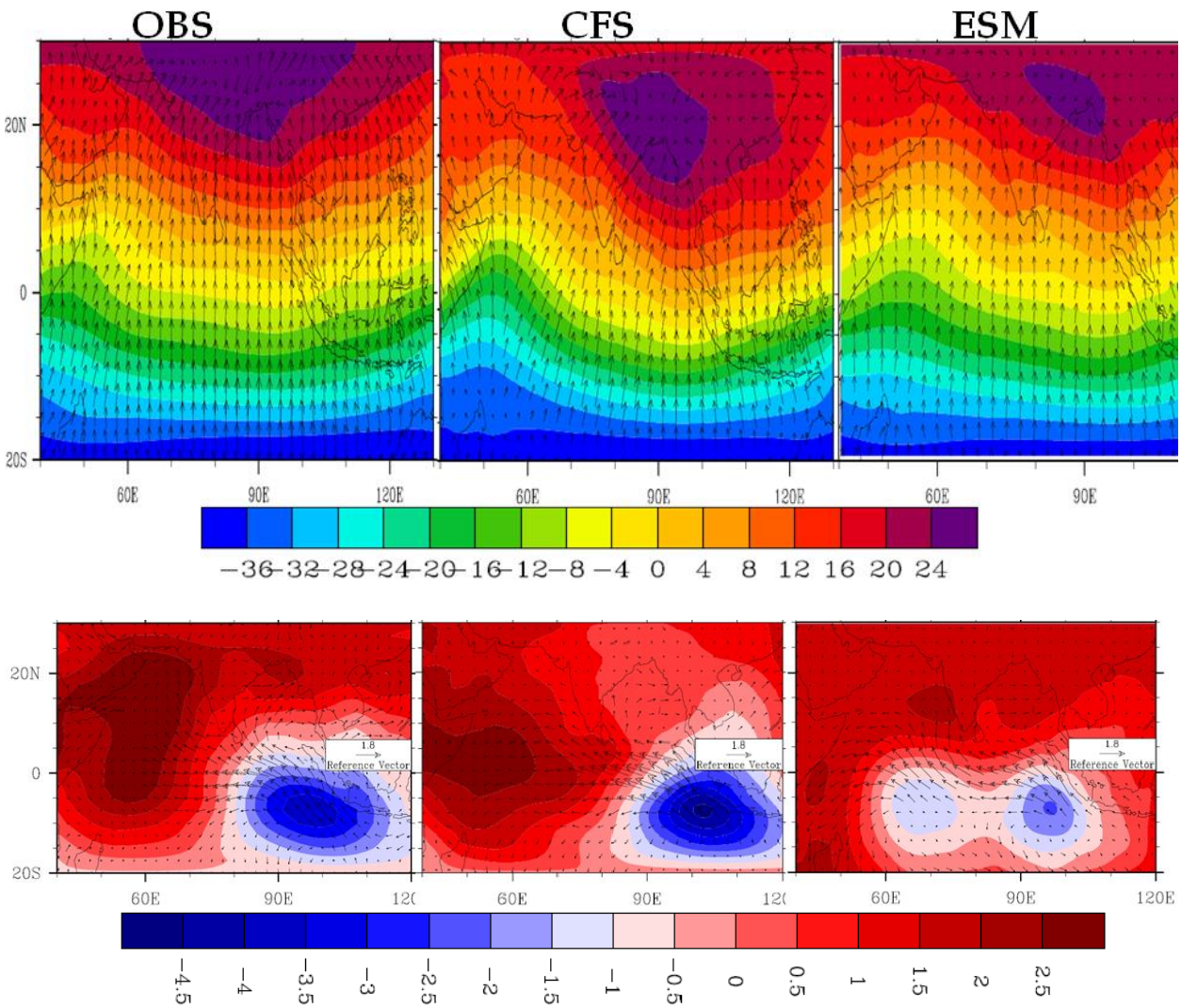


Fig 32: Top panel:- mean velocity potential (VP) for JJAS structure (a) Observations (b) CFS (c) ESM. Bottom panel:- Composite of VP anomalies for JJAS of positive IOD events for observation, CFS and ESM respectively (from left to right).

The winds always move towards the areas of convergence. So the velocity potential was calculated for the divergent part of the winds at 925 hPa. From the Fig 32, the mean velocity potential during JJAS in the observations shows a clear larger convergence is in the northern part of India. And the area is spread out to a great extent (purple color). But the models are not able to capture it properly. Though the pattern remains same, the convergent center is shifted to north-east, and is also contracted from the observations. In ESM, it is further disrupted, with the

pattern bending towards North East and the convergent center further shrunken. The wind vectors show that the winds are consistently following the convergent centers.

A composite of velocity potential anomalies was produced for the positive IOD events for the months of JJAS (Fig. 32). There are differences between the observations and model simulations. The convergent center in case of observation is spread in the Western Indian Ocean and extends up to the continent. And the divergent end is located at the SEIO. In case of CFS the pattern remains similar, but the convergent center is only strong in the WIO, it is not reaching the continent. In case of ESM, there is an entirely different structure. There is a dumbbell shaped structure for the divergent area. And this structure covers the entire IO just below the equator. There are two centers in this shape; one is a strong divergent structure, whereas the other is weak. Moreover, there is no center for strong convergence neither in the ocean nor in the land.

The winds vectors in the observations are moving from the divergent center to the convergent center, and thus inland. However in the models, there are no winds to the land, the winds start in the ocean and converge in the ocean itself. Both in CFS and ESM, there are very strong winds diverging and converging, but very weak winds move over the land. This might be the reason being weak and negative correlation between the IOD and ISMR, as there is no passage for the transport of moisture possible.

## Chapter 6: Discussion

This study, in large part, was spent on evaluating the IOD events simulated in the climate simulations of 100 years long using CFSv2 and ESM. The study stresses on the point that the mean state of the ocean should be resolved properly for an accurate climate simulations using coupled models. While validating the model, it is seen that both CFS and ESM reasonably reproduce the surface features in terms of IOD. However, the differences are visible in the frequency of such event. There exist even a 'spurious' mode of IOD-like evolution in the early part of the year in both the CFSv2 and ESM.

The EOF of SST gives a clear indication that the models are capturing the features properly. There is slight discrepancy in ESM, as the location of polarities seems to be a bit shifted, but the pattern is quite close to that of observation, with the basin wide warming in the first mode, and dipole in the second mode. The dominant modes of inter-annual variability in the Indian Ocean do not show co-variability between the surface and the subsurface. In contrast to the SST variability dominated by the El Niño and Southern Oscillation (ENSO), subsurface variability is governed by the Indian Ocean Dipole (IOD) in the Tropical Indian Ocean (Rao and Behera 2005). The result obtained is in consensus as no basin wide signal is present in the EOF of subsurface features such as thermocline.

The model EOFs of subsurface ocean such as thermocline and dynamic height captured a trend signal mostly of origin related to deeper ocean spin-up which was going on even after a simulation of 100 years. In the case of ESM the trend is visible in the thermocline as EOF-1 mode, whereas in the case of CFSv2, it is seen in the dynamic height EOF-1. These two EOFs, one in ESM and other in CFS, are probably also due to the biases building up in the interior of

the ocean. In case of ESM, since the increasing trend is only present in the thermocline, and not in the dynamic height it is understood that either the bias is developing only at the thermocline or there are biases both at the thermocline and deeper depths, but when the integration for dynamic height is carried out, they cancel out, and so do not appear.

The major finding of this work is the role of oceanic biases in the surface ocean dynamics such as IOD. The temperature profile clears that there is significant cold bias at the surface in both the models, and deeper warmer bias. With the present level of analysis it is hard to associate a reason for such model biases, but could most likely due to the biases in the seasonal surface vertical mixing. Further works are required to see how the biases are developing in the interior ocean.

The role of oceanic biases in the surface dynamics such as IOD simulated in the models appears to have high frequency oscillations. And many events are occurring in the earlier part of the year. In the observations, the events take place from June to Dec, but in the models they are also present in Jan-May.

Vinayachandran et al. (2002) demonstrated that that during the positive IOD events the easterly wind anomalies along the equator excite an upwelling Kelvin wave along the equator. This Kelvin wave, on reaching the eastern boundary, lifts the thermocline in the eastern equatorial Indian Ocean and reflects as an upwelling Rossby wave which propagates westward. The upwelling Rossby wave propagates westward moving the cold SST anomalies west- ward along the equatorial Indian Ocean. McCreary et al (1993) also quoted that the Kelvin and Rossby waves play an important role on the seasonal dynamics and thermodynamics of the tropical Indian Ocean, particularly in the equatorial and coastal regions. Therefore the biases in the model

ocean interior and thereby bias in the baroclinic speed probably affect the dynamics governing the events, and so cause a change in the frequency.

Recent studies using coupled model projects show that IOD intensity and positive IOD frequencies may increase in the warming climate. Such projection are basically based on the coupled ocean simulation where in the deeper ocean biases are inherent. Our study shows that climate models should be optimized to reduce the bias in the mean state of the ocean. This has larger implications even in resolved coupled ocean-atmosphere phenomenon such as IOD.

The sensitivity experiments are done with a 3-1/2 layer reduced gravity model shows that when observed winds are forced upon the CFS and observed stratification, a noisy signal were obtained, and when the model winds are forced upon the observed stratification there also noisy signal were obtained. This suggests that both stratification and winds are playing a role in creating the noise. However, the noisiness from the CFS winds is higher than from the observed winds. It can be said that the winds are the noisy and create high frequency, and the stratification enhances the effect. A close look at the power spectrum of the noises further approves, as the dominant peak in case of CFS winds has higher frequency.

The hypothesis of short term intensification of feedback, due to faster dispersion speed is suggested, but needs to be checked for the time scales of each process concerned. The oscillatory nature of noises in the model solution is hypothesized as associated with the biased normal mode structure of the model ocean. The analytical solution to support this argument shows that there can be a periodic solution if the feedback is negative. A possible candidate for negative feedback is SST-moisture feedback. This has been associated to explain the ‘short term intensification of feedback’ in the early part of the year in the model. However, further studies are required to

prove this. Also the role of pre-conditioning may be crucial for perturbation to grow positively. At least in the early part of the year such pre-conditioning perhaps is not happening.

It is still unclear that what originates the noisy perturbation in the model. Because they are strongly phase-locked to winter months, this can be of Madden Julian Oscillation (MJO) related wind perturbations. According to a recent study (Zhou et al. 2011), if the physics, in terms of the parameterizations are improved, there is significant improvement in the MJO simulation. A similar modification is necessary for our models. There is a lot of scope for improvement in the models, which is possible if the thermodynamics, mechanics and dynamics of the model are studied in details; also important is the air sea coupling which can change drastically with a slight tuning. This is presently out of the scope of our study. In a commendable research by (Achuthavarier et al. 2011) , the failure of model at representing a correlation is worked upon. Such studies can help in bringing a prescription for CFS and ESM.

As concerned with the relationship of IOD and monsoon, very weak correlation coefficients are obtained. (Ashok and Saji, 2007) also reported similar weak correlation. However, when monthly correlation analysis was done, it is seen that not much improvement is obtained. (Ashok and Saji, 2007), show that there is positive correlation at least in the month of July. This might be not visible in our study, probably because they have taken a partial correlation in their analysis, removing the effect of ENSO, but the same has not been done here.

The mean state of velocity potential in JJAS shows that both the model is unable to capture the convergence center properly; this might be causing a negative correlation. Also, the composite of velocity potential anomalies shows that there is no pathway for the moisture to enter the land. All this adds to the weak or negative correlation we obtain in CFS.

The focus of our study was to see what roles do the model biases play, and how do they govern the dynamics. In a very recent study by Cai et al., (2013, Nature) it is reported that a reduction in the difference in amplitude between positive and negative dipole events is expected as a, long term climate projection. This is in response to global warming, where the mean temperature will increase and so the difference decreases. However, this may be only partially true. Since the model biases have been ignored in the above study, there is a possibility that this might be due to the model biases, as we have seen that they play an important role. Also, there may be a change in the frequency, intensity and duration of the event in the climate projections due to model biases, rather than global warming. This requires minimization of the biases by improving physics.

## Conclusion

The Indian Ocean Dipole Mode is studied in the Coupled Forecast System model and the Earth System Model. It is seen that the surface features reproduced in both the models are quite reasonable. However, there is a discrepancy in the frequency of events between observations and the models. It is seen that there are a number of events occurring in the models in the earlier part of the year (Jan-May), when the actual season for the phenomenon is June–Dec. Also, the time series for the EOF of SSTA are noisy in models. It is found that ocean model biases contribute to this increased frequency. It is seen that in the model due to wrong stratification, there is faster dispersion of baroclinic waves. Sensitivity studies show that the equatorial winds are noisy, and the stratification further adds to that noise. A hypothesis is suggested, according to which the faster dispersion causes a negative feedback to develop and the event persists for a short time even in the absence of preconditioning.

The correlation between Indian Summer Monsoon Rainfall and Dipole Mode Index is weak in observations. But the models have negative to weak correlation. The velocity potential mean state and anomalies show that the pathway for the moisture to reach land is absent in the models, and convergent center is not captured properly. This weak correlation might be attributed to this missing path or the ENSO effect, but the effect of biases cannot be ignored.

In case of climate projections, it is possible that if these model biases are ignored it might lead to a wrong interpretation of the changed frequency, or duration and other characteristics of such a dominant mode of variability, to the trend of global warming rather than model biases. Thus a proper prescription for the improvement of models is necessary, in terms of climate changes to be predicted. In seasonal forecast, the model simulation does not seem to be much affected by the biases.

## Acknowledgement

I am thankful for the guidance provided by Dr. Vinu Valsala, Dr. Swapna Panickal and Dr. Roxy Mathew Koll for the guidance during the project duration. I am highly thankful to Dr. Rajib Chattopadhyaya for the technical discussions. I also thank Prof. B.N. Goswami, Director, IITM for facilitating this research as part of CAT-ESSC training program. Also, Dr. R.H.Kripalani is thanked for the encouragement and support throughout. And last but not the least; I thank all my colleagues at IITM for their unending co-operation and help. It would not have been possible without them.

## References:


Achuthavarier, D., V. Krishnamurthy, B. P. KIRTMAN, and B. HUANG, 2011: Role of the Indian Ocean in the ENSO – Indian Summer Monsoon Teleconnection in the NCEP Climate Forecast System. *J. Clim.*, **25**, 2490–2508, doi:10.1175/JCLI-D-11-00111.1.

Annamalai, H., R. Murtugudde, J. Potemra, S. P. Xie, P. Liu, and B. Wang, 2003: Coupled dynamics over the Indian Ocean : spring initiation of the Zonal Mode. *Deep sea Res. part II*, **50**, 2305–2330, doi:10.1016/S0967-0645(03)00058-4.

Annamalai, H., S. P. Xie, J. P. McCreary, and R. Murtugudde, 2004: Impact of Indian Ocean Sea Surface Temperature on Developing El Niño *. *J. Clim.*, **18**, 302–319.

Ashok, K., 2003: A Look at the Relationship between the ENSO and the Indian Ocean Dipole. **81**, 41–56.

Ashok, K.,, Guan, Z., Saji, N. H., and Yamagata, T., 2004a: Individual and combined influences of the ENSO and Indian Ocean Dipole on the Indian summer monsoon, J. Climate, 17, 3141-3155.

Ashok, K., and N. H. Saji, On Impacts of ENSO and Indian Ocean Dipole events on the sub-regional Indian summer monsoon rainfall.

Ashok, K., and N. H. Saji, 2007: On the impacts of ENSO and Indian Ocean dipole events on sub-regional Indian summer monsoon rainfall. *Nat. Hazards*, **42**, 273–285, doi:10.1007/s11069-006-9091-0. http://link.springer.com/10.1007/s11069-006-9091-0 (Accessed December 10, 2013).

Ashok, K., Z. Guan, and T. Yamagata, 2001: Impact of the Indian Ocean Dipole on the Relationship between the Indian Monsoon Rainfall and ENSO. *Geophys. Res. Lett.*, **28**, 4499–4502.

Ashok, K., W. Chan, T. Motoi, and T. Yamagata, 2004: Decadal variability of the Indian Ocean dipole. **31**, 3–6, doi:10.1029/2004GL021345.

Bjerknes, J., 1969. Atmospheric teleconnections from the equatorial Pacific. Monthly Weather Review 97, 163–172.

Cai, W., X.-T. Zheng, E. Weller, M. Collins, T. Cowan, M. Lengaigne, W. Yu, and T. Yamagata, 2013: Projected response of the Indian Ocean Dipole to greenhouse warming. *Nat. Geosci.*, **6**, 999–1007, doi:10.1038/ngeo2009. http://www.nature.com/doifinder/10.1038/ngeo2009 (Accessed November 29, 2013).

Carton JA, Giese BS (2008) A reanalysis of ocean climate using Simple Ocean Data Assimilation (SODA). Month Weather Rev 136:2999–3017

Dee DP et al (2011) The ERA-Interim reanalysis: configuration and performance of the data assimilation system. Q J R Meteorol Soc 137:553–597

Delworth, T. L., A. Broccoli, R. J. Stouffer, and K. W. Dixon, 2006: GFDL ' s CM2 Global Coupled Climate Models . Part I : Formulation and. *Am. Meterological Soc.*, **19**, 643–674.

Delworth et al, (2011) Distinguishing the roles of natural and anthropogenically forced decadal climate variability, Bull. Am. Meteorol. Soc

Dunne, J. P., R. a. Armstrong, A. Gnanadesikan, and J. L. Sarmiento, 2005: Empirical and mechanistic models for the particle export ratio. *Global Biogeochem. Cycles*, **19**, n/a–n/a, doi:10.1029/2004GB002390. http://doi.wiley.com/10.1029/2004GB002390 (Accessed Nov ember 8, 2013).

Fischer, A. S., P. Terray, E. Guilyardi, and S. Gualdi, 2005: Two Independent Triggers for the Indian Ocean Dipole / Zonal Mode in a Coupled GCM. *J. Clim.*, **18**, 3428–3449.

Gill A.E. 1982. Atmosphere-Ocean Dynamics. New York: Academic Press.

Gill, A. E. (1980). Some simple solutions for heat-induced tropical circulation. Quarterly Journal of Royal Meteorological Society, 106, 447-462

Gadgil, S., P. N. Vinayachandran, P. A. Francis, and S. Gadgil, 2004: Extremes of the Indian summer monsoon rainfall , ENSO and equatorial Indian Ocean oscillation. **31**, 2–5, doi:10.1029/2004GL019733.

Iizuka, S., T. Matsuura, and T. Yamagata, 2000: The Indian Ocean SST dipole simulated in a coupled general circulation model. Geophys. Res. Lett., 27, 3369–3372

IPCC (2013) IPCC WGI fifth assessment report, chapter 2— observations: atmosphere and surface

Izumo, T. and Coauthors, 2010: Influence of the state of the Indian Ocean Dipole on the following year ' s El Niño. *Nat. Geosci.*, **3**, 168–172, doi:10.1038/ngeo760. http://dx.doi.org/10.1038/ngeo760.

Kalnay, E., et al. (1996), The NCEP/NCAR 40 year reanalysis project, Bull. Am. Meteorol. Soc., 77, 437 – 471.

Kripalani, R. H., and A. Kulkarni, 1994: Climatic impact of El Nino / La Nina on the Indian monsoon :A new perspective. *Weather*, **52**, 205–209.

Kundu, P. K., and J. S. Allan, Some three dimensional character- istics of low-frequency current fluctuations near the Oregon coast, J. Phys. Oceanogr., 6, 181-199, 1976.

McCreary, J.P., Kundu, P.K., Molinari, R., 1993. A numerical investigation of the dynamics, thermodynamics and mixed layer processes in the Indian Ocean. Progress in Oceano- graphy 31, 181–244

Parthasarathy, B., Kumar, R. K., and Munot, A. A.: 1994: All-India monthly and seasonal rainfall series: 1871-1993. Theor. Appl. Climatol., 49, 217-224.

Rao, S. A, S. K. Behera, Y. Masumoto, and T. Yamagata, 2002: Interannual variability in the subsurface tropical Indian Ocean with a special emphasis on the Indian Ocean dipole. Deep-Sea Res. II, 49, 1549–1572

Rao, S. A., and T. Yamagata, 2004: Abrupt termination of Indian Ocean dipole events in response to intraseasonal disturbances. *Geophys. Res. Lett.*, **31**, 1–4, doi:10.1029/2004GL020842.

Rao, S. A., and S. K. Behera, 2005: Subsurface influence on SST in the tropical Indian Ocean : structure and interannual variability. *Dyn. Atmos. Ocean.*, **39**, 103–135, doi:10.1016/j.dynatmoce.2004.10.014.

Saha, S., S. Moorthi, X. Wu, J. Wang, and S. Nadiga, 2010: The NCEP Climate Forecast System Reanalysis. 1015–1057, doi:10.1175/2010BAMS3001.1.

Saji, N. H., and T. Yamagata, 2003: Possible impacts of Indian Ocean Dipole mode events on global climate. *Clim. Res.*, **25**, 151–169.

Saji, N. H., B. N. Goswami, P. N. Vinayachandran, and T. Yamagata, 1999: A dipole mode in the tropical Indian Ocean. *Nature*, **401**, 360–363.

Schott, F. A., and J. P. M. Jr, 2001: The monsoon circulation of the Indian Ocean. **51**, 1–123.

Servain, J., and D. M. Legler, 1986: Empirical orthogonal function analyses of tropical Atlantic sea surface temperature and wind stress: 1964-1979. *J. Geophys. Res.*, **91**.

Su, H., J. D. Neelin, and C. Chou, 2001: Tropical teleconnection and local response to SST anomalies during the 1997-1998 E1 Nifio. *J. Geophys. Res.*, **106**, 20025–20043.

Trenberth, K. E., 1997: The Definition of El Niño. *Bull. Am. Meteorol. Soc.*,.

Valsala, V., 2008: First and Second Baroclinic Mode Responses of the Tropical Indian Ocean to Interannual Equatorial Wind. *J. Oceanogr.*, **64**, 479–494.

Vinayachandran, P. N., S. Iizuka, and T. Yamagata, 2002: Indian Ocean dipole mode events in an ocean general circulation model. *Deep sea Res. part II*, **49**, 1573–1596.

Vinayachandran, P. N., P. A. Francis, and S. A. Rao, 2006: Indian Ocean Dipole : Processes and impacts. 569–589.

Webster, P. J., A. M. Moore, J. P. Loschnigg, and R. R. Leben, 1999: Coupled ocean ± atmosphere dynamics in the Indian Ocean during 1997 ± 98. *Nature*, **401**, 356–360.

Yamagata, T., S. K. Behera, S. A. Rao, Z. Guan, K. Ashok, and N. H. Saji, 2003: Comments on "Dipoles, Temperature Gradients, and Tropical Climate Anomalies." *BAMS*, 1999–2003.

Zheng, X. T., and S. Xie, 2009: Indian Ocean Dipole Response to Global Warming : Analysis of Ocean – Atmospheric Feedbacks in a Coupled Model *. *J. Clim.*, **23**, 1240–1253, doi:10.1175/2009JCLI3326.1.

Zhou, L., R. B. Neale, M. Jochum, and R. Murtugudde, 2011: Improved Madden – Julian Oscillations with Improved Physics : The Impact of Modified Convection Parameterizations. *J. Clim.*, **25**, 1116–1136, doi:10.1175/2011JCLI4059.1.

## Reviews

Major comments

Figure 21 clearly shows that both case 3 and case 4 show similar spatial and temporal structure. Suggesting that it is the winds rather than stratification is responsible for the spurious high frequency variability in IOD time series.

Reply:

Model stratification has been used in Case 3, and observed stratification in Case 4, with observed winds in both. The spatial structure for the EOF performed on SSH in both the cases is very similar, but the temporal variability of Case 3 has noise build in it as compared to that of Case 4.The smoothening of the time series from Case 3 to case 4 is very significant. And in case 1 & Case 2, it is seen that model winds also bring in a lot of noise. So, it is not exact enough to conclude that only winds are bringing in the noise. The stratification has a role in it as well.

Minor comments

EOF analysis is very sensitive to spatial domain considered for analysis. For observations and CFS the domain 30°-130°E is used, while for ESM 30°-120°E is used.

Reply:

The maps were rechecked using the same spatial domain. It does not bring any significant changes. Most of the processes affect the Indian Ocean Domain from 50E -110 E, and since it is common in both the models and observations, changing the domain other than the most sensitive area did not bring any crucial change in EOF spatial maps.